Protein Folding Determinants: Structural Features Determining Alternative Disulfide Pairing in α- and χ/λ-Conotoxins[†,‡]

Tse Siang Kang,[#] Zoran Radić,[◊] Todd T. Talley,[◊] Seetharama D. S. Jois,[§,||] Palmer Taylor,[◊] and R. Manjunatha Kini*[,#,⊥]

Protein Science Laboratory, Department of Biological Sciences, and Department of Pharmacy, Faculty of Science, National University of Singapore, Singapore 117 543, Department of Pharmacology, Skaggs School of Pharmacy & Pharmaceutical Sciences, University of California at San Diego, La Jolla, California 92093, and Department of Biochemistry, Medical College of Virginia, Virginia Commonwealth University, Richmond, Virginia 13298

Received September 21, 2006; Revised Manuscript Received December 1, 2006

ABSTRACT: α-Conotoxins isolated from *Conus* venoms contain 11−19 residues and preferentially fold into the globular conformation that possesses a specific disulfide pairing pattern (C_{1-3}, C_{2-4}). We and others isolated a new family of χ-conotoxins (also called λ conotoxins) with the conserved cysteine framework of α-conotoxins but with alternative disulfide pairing (C_{1-4}, C_{2-3}) resulting in the ribbon conformation. In both families, disulfide pairing and hence folding are important for their biological potency. By comparing the structural differences, we identified potential structural determinants responsible for the folding tendencies of these conotoxins. We examined the role of conserved proline in the first intercysteine loop and the conserved C-terminal amide on folding patterns of synthetic analogues of ImI conotoxin by comparing the isoforms with the regiospecifically synthesized conformers. Deamidation at the C-terminus and substitution of proline in the first intercysteine loop switch the folding pattern from the globular form of α-conotoxins to the ribbon form of χ/λ-conotoxins. The findings are corroborated by reciprocal folding of CMrVIA χ/λ-conotoxins. Substitution of Lys-6 from the first intercysteine loop of CMrVIA conotoxin with proline, as well as the inclusion of an amidated C-terminal shifted the folding preference of CMrVIA conotoxin from its native ribbon conformation toward the globular conformation. Binding assays of ImI conotoxin analogues with *Aplysia* and *Bulinus* acetylcholine binding protein indicate that both these substitutions and their consequent conformational change substantially impact the binding affinity of ImI conotoxin. These results strongly indicate that the first intercysteine loop proline and C-terminal amidation act as conformational switches in α- and χ/λ-conotoxins.

The venoms of marine predatory cone snails contain cocktails of pharmacologically active peptides. These *Conus* peptides are broadly classified into two groups: (a) possessing a single or no disulfide bridge and (b) having multiple disulfide bridges. The latter group forms the major components of the *Conus* venom (*1*). These peptides, collectively named as conotoxins, form compact and well-ordered three-dimensional (3D) structures through the formation of two or more disulfide bridges among the short sequence length of 10−30 amino acid residues (*1*−*3*). So far, an extensive listing of conotoxins have been purified and characterized. Depending on the characteristic disulfide linkage patterns seen in the mature peptides as well as the highly conserved signal sequences of the precursor molecules, these toxins are classified into the A-, M-, O-, P-, S-, and T-superfamilies (*2*). On the basis of their cysteine framework, the first three superfamilies are subdivided into various families. Members of each family of conotoxins possess identical cysteine framework as well as remarkable molecular specificity to recognize a precise subclass of ion channels/receptors (*1*−*3*).

α-Conotoxins, which belong to the A-superfamily, are one of the most intensely studied groups of conotoxins. Functionally, they are competitive inhibitors of either "muscle-type" or "neuronal-type" nicotinic acetylcholine receptors (*2*). Structurally, α-conotoxins possess 11−19 amino acid residues including four highly conserved cysteine residues and fold into the native globular conformation, with a specific

[†] This work is supported by Biomedical Research Council, Agency for Science and Technology, Singapore, and NIH Grant GM18360.

[‡] Coordinates of the calculated solution structures for all peptide variants described in this manuscript have been deposited with the following Protein Data Bank codes: CMrVIA K6 Amide: 2IHA; CMrVIA P6 Amide: 2IH7; CMrVIA P6 Acid: 2IH6; CMrVIA K6 Acid: 2B5P (PDB code released in an earlier publication); ImI A6 Amide: 2IFI; ImI P6 Acid: 2IGU; ImI K6 Acid: 2IFJ; ImI K6 Amide: 2IFZ.

* To whom correspondence to should be addressed at Protein Science Laboratory, Department of Biological Sciences, Faculty of Science, National University of Singapore, Singapore 117 543. Tel: (65) 6516-5235. Fax: (65) 67792486. E-mail: dbskinim@nus.edu.sg.

[#] Protein Science Laboratory, Department of Biological Sciences, National University of Singapore.

[§] Department of Pharmacy, Faculty of Science, National University of Singapore.

[◊] University of California at San Diego.

[⊥] Virginia Commonwealth University.

[||] Current address at Department of Pharmaceutical Sciences, College of Pharmacy, University of Louisiana at Monroe, Monroe, LA 71209-0470.

10.1021/bi061969o CCC: $37.00
Published on Web 02/22/2007

cysteine pairing (C_{1-3}, C_{2-4}). In contrast, the two non-native forms (which suffer at least a 10-fold reduction in biological activity) are not found in nature (*4*).

To determine the contribution of the side chains toward the formation of the globular conformation, Zhang and Snyder studied the effect of alanine substitution on several conserved residues in the 3/5 α-conotoxin GI (*5*). However, substitution with alanine, either singly or in combination, failed to result in the total conformational switch from the native conformation to either of the two non-native forms. Substitutions included proline and glycine that are likely to induce a kink or flexibility in the sequence and often dictate folding patterns (*6*, *7*). The influence of the number of residues within the intercysteine loops was also examined by changing the position of the third cysteine residue in the peptide sequence. The authors concluded that for α-conotoxin sequences with intercysteine loops comprising less than five residues number rather than type of residues was more critical for achieving a globular conformation; loops with an even number of residues appeared to favor the globular conformation (*5*). However, this rule does not appear applicable to the different subclasses of α-conotoxin, especially in the prediction of the globular versus the ribbon conformations (*8*).

Recently, several groups discovered a new family of conotoxins: χ-conotoxins (or λ-conotoxin) (*9*−*11*). This novel class of conotoxins possesses the conserved arrangement of quadruple cysteines as α-conotoxins. However, their native cysteine pairing is unique as they exhibit a ribbon (C_{1-4}, C_{2-3}) conformation instead of the usual globular structure seen in α-conotoxins. The mechanism of neurotoxicity induced by the χ/λ-conotoxins is also distinct from that of α-conotoxins (*10*). As in the case of α-conotoxins, the native cysteine pairing and consequent conformation have also been shown to be important for the biological activity of χ/λ-conotoxins: the non-native globular isoform of χ/λ-conotoxin CMrVIA displays a lower potency of three orders in magnitude in the induction of seizures in mice (*9*). These findings underscore the crucial role of disulfide linkages and conformation for the biological potencies of these peptides. However, the structural features governing the disulfide pattern and attendant conformational differences are still unclear.

The discovery of χ/λ-conotoxins lends insights into the structural features that are critical for the differing folding patterns of these two families of *Conus* peptides. To delineate structural determinants responsible for the shift in folding tendency, we systematically analyzed the structural differences between α-conotoxins and χ/λ-conotoxins. Herein we describe the contribution of the proline residue in the first intercysteine loop in affecting the folding pattern in representative members of these families of conotoxins. By examining further variants, we also confirm our earlier finding on the effect of C-terminal amidation on the folding pattern of ImI α-conotoxin (*12*). By using synthetic congeners of ImI conotoxin and parallel NMR studies of the various folded forms, we show that these structural determinants, individually and in combination, shift the pattern toward the globular conformation. These structural changes of various ImI conotoxin analogues are correlated with their ability to bind to *Aplysia* and *Bulinus* acetylcholine binding proteins (abbreviated as A-AChBP and B-AChBP, respectively), the protein family of which structures of α-conotoxins at their binding sites have been reported (*13*, *14*). In turn, by substituting proline into the first intercysteine loop of CMrVIA χ/λ-conotoxin, we show that the native ribbon conformation of CMrVIA conotoxin reciprocally folds into its non-native globular form.

MATERIALS AND METHODS

Materials. Standard Fmoc-L-amino acid hydroxyl derivatives, Fmoc-L-Cys(Trt)-PEG-PS (polyethylene glycol-polystyrene) support resin, Fmoc-PAL-PS support resin, *N*,*N*-dimethylformamide (DMF), trifluoroacetic acid (TFA), 20% piperidine in DMF, *O*-(7-azabenzotriazol-1-yl)-1,1,3,-3-tetramethyluronium hexafluorophosphate (HATU), and *N*,*N*-diisopropylethylamine (DIPEA) were purchased from Applied Biosystems Asia Pte Ltd (Foster City, CA). Fmoc-L-Cys(Trt)-OPfp amino acid derivative was purchased from Novabiochem (San Diego, California). Vydac C18 90 Å (4.6 × 250 mm) column and Jupiter 300 5 μ C18 300 Å (10 × 250 mm) semipreparative column were purchased from Grace Vydac (Hesperia, California), and Phenomenex (Torrance, California), respectively. 1,2-Ethanedithiol and thioanisole were obtained from Fluka/Riedel-de Haën (Sigma Aldrich, St. Louis, Missouri). All other chemicals and reagents used were of analytical grade.

Peptide Synthesis and Characterization. For ease of comparison, native ImI α-conotoxin and CMrVIA χ/λ-conotoxin shall be referred as ImI P6 Amide and CMrVIA K6 Acid, respectively. Except for CMrVIA P6 Amide and CMrVIA P6 Acid variants which were custom synthesized by Mimotopes (Melbourne, Australia), analogues of ImI conotoxin and CMrVIA conotoxin (Table 2) were chemically synthesized on an ABI Pioneer model 433A Peptide synthesizer using 9-fluorenylmethoxycarbonyl (Fmoc) chemistry.

The amino acid residues were coupled using *O*-(7-azabenzotriazol-1-yl)-1,1,3,-3-tetramethyluronium hexafluorophosphate/ *N*,*N*-diisopropylethylamine for in situ neutralization chemistry. Peptides with C-terminal amidation were synthesized using Fmoc-PAL-PS (5-(aminomethyl-3,5-dimethoxy-phenoxy) valeric acid linker) support, while variants with a free carboxyl terminal were assembled on a preloaded Fmoc-L-Cys(Trt)-PEG-PS (4-hydroxymethylphenoxyacetic acid linker) support resin.

Selective deprotection involving orthogonal side chain protection of the four cysteine residues generated specific cysteine pairings in the formation of the two disulfide bridges (*9*). Cysteine pairs involved in the formation of the first and second disulfide bridge were protected using S-trityl and S-acetamidomethyl protection groups respectively. Peptides designed for folding and oxidation studies were synthesized with all four cysteine residues protected with an S-trityl group followed by its removal in the resin cleavage step.

The assembled peptides were cleaved from the resin by incubating with cleavage cocktail comprising of TFA/1,2-ethanedithiol/thioanisole/water (90:4:4:2% v/v) for 2 h. The crude peptides were then purified using a Jupiter 300 Å 5 μ C18 (10 × 250 mm) semipreparative column on an ÄKTA purifier system. Molecular masses were ascertained by electrospray ionization mass spectrometry (ESI-MS) on a Perkin-Elmer Sciex API III Triple-stage Quadrupole system.

Iodine Oxidation. Peptide variants with the desired regiospecifically synthesized disulfide linkage were generated by means of a two-step oxidation process through selective deprotection. The first disulfide bond was formed between the two S-trityl protected cysteine residues which were deprotected during the cleavage step. This oxidation was achieved by stirring 0.1 mg/mL of peptide solution in 0.1 M NH_4HCO_3 (pH 8.5) in air. Complete oxidation of the first disulfide bridge was confirmed by the reduction of two mass units as determined with ESI-MS.

The second pair of cysteines with S-acetamidomethyl groups was deprotected and concomitantly oxidized by adding 0.1 M I_2 solution to a deaerated solution containing 0.1 mM peptide (10 equiv/ACM) in acetonitrile/TFA/water (20:2:78% v/v) and stirred vigorously under nitrogen blanket for 5 min before quenching with 1 M ascorbic acid dropwise until the solution becomes colorless. The crude peptides were purified to >90% purity by semipreparative reverse-phase HPLC (data not shown) and characterized by ESI-MS. The observed mass for all peptides matched the theoretical mass well (Supplementary Table S1, Supporting Information). The purified reduced peptides were then lyophilized and stored at −20 °C.

Oxidation/ Folding Studies. The molecular masses and integrity of fully deprotected and reduced peptides were verified using ESI-MS prior to oxidation studies. Oxidation/ folding studies were conducted using either glutathione redox system or air oxidation in the folding buffer (100 mM Tris-HCl and 2 mM EDTA, adjusted to pH 8.5) with or without denaturant (6 M guanidium HCl). For air oxidation, 0.1 mM of peptide was dissolved in buffer solution and allowed to stir in air for 48 h. Glutathione oxidation was performed using reduced/oxidized glutathione system (0.8 mM GSSG/ 1.6 mM GSH) incubated under nitrogen blanket for 4 h. Air oxidation will provide cleaner products with few side reaction products, but they are not likely to represent the energetically favorable conformations. The glutathione redox system provides an oxidative environment that drives oxidation of the peptides to completion, favoring the kinetically stable conformations. However, this system is also more likely to result in side reaction products as compared to air oxidation (*5*). Oxidations in both sets of conditions were done in triplicate and repeated in both folding buffer and denaturing buffer.

Oxidation reactions were quenched by adding glacial acetic acid to adjust pH to 4.0 before separation and quantification on a Vydac (4.6 × 250 mm) 90 Å C18 column (*5*). The oxidized peptides were separated using a gradient of 80% acetonitrile, with either 0.1% TFA or formic acid as ion-pairing agent over 100 min. Elution of peptides was monitored by absorbance at 215 and 280 nm and quantified by peak areas.

NMR Studies. Samples for NMR spectroscopy were prepared in 90% H_2O/10% D_2O to concentrations of ∼2 mM peptide before correcting its pH to 3.1 using deuterated sodium hydroxide and deuterium chloride. Proton 1D spectra were acquired at various temperatures ranging from 290 to 310 K, and the temperatures achieving the best resolution were used for the 2D experiments. All spectra acquired were referenced to 4,4-dimethyl-4-silapentane-1-sulfonate (DSS) as the internal standard. TOCSY experiments (*15*) were carried out with a mixing time of 80 ms, and ROESY experiments (*16*) were conducted at 300 ms. All 2D NMR spectra were acquired on a Brüker AVANCE DRX 500 MHz spectrometer with GRASP-II facility, with BVT 3000 control unit, maintaining the temperature within ±0.1 K. Water suppression in the 2D spectra was achieved using a modified watergate sequence (*17*), and spectra were acquired using time proportional phase incrementation. Spectra were acquired with 2048 and 512 data points in F2 and F1 respectively, multiplied with squared sine bell window functions shifted by 90°, before zero-filling to 2048 by 1024 data points. The spectra were then processed on Silicon Graphics Fuel Workstation using Brüker XWIN−NMR software or Mestre-C: 4.5.9.1 software on Microsoft Windows platform.

Molecular Modeling. Molecular modeling studies were carried out using InsightII 2000 software (Accelrys Inc., San Diego, CA) on an Origin 2000 Silicon Graphics computer, using consistent valence force field (Cvff) in the calculations. Conformational spaces consistent with the experimental ROE constraints derived from the NMR spectrum were examined in vacuo. ROE intensities were classified as strong (1.9−3.1 Å), medium (1.9−3.8 Å), and weak (1.9−5.0 Å). The protons were brought to observable ROE distances using a penalty force of 100 kcal mol^{-1} $Å^{-2}$. After the initial energy minimization and molecular dynamics at 300 K, the distance versus time plot between the thiol groups of the four cysteine groups was generated. The conformation satisfying the following condition of disulfide bridge criteria was manually bridged to form the two disulfide bonds. The distance between two sulfur atoms after the disulfide bond formation should be in the range of (r_{ss}) 1.8−2.4 Å and dihedral angle $\chi_{ss} = |70 - 100°|$. The conformation with the shortest distance between the two pairs of cysteines corresponding to the expected conformation was manually bridged to form the two disulfide bonds. Partial charges and potentials were fixed using InsightII with Cvff force field. High-temperature molecular dynamics was then performed using InsightII Discover module at 300 and 600 K at 10 ps, followed by 900 K at 20 ps with trajectories updated every 100 fs. Molecular dynamics studies were subsequently done at decreasing temperatures from 900 to 400 K in steps of 100 K before cooling to 300 K by "soaking" in an assembly of water molecules for 20 ps (sphere radius of 8 Å). At each point of the high-temperature simulations, all peptide bonds (except proline residues) were held in the trans position. Pseudo-atom corrections were made for methyl and methylene protons according to Wuthrich et al. (*18*). A total of 211 structures were generated, of which, the 15 frames with the lowest energy levels were relaxed using steepest descent method by subjecting to 100 steps of energy minimization, followed by conjugate gradient until the root-mean-square derivative was less than 0.6 kcal mol^{-1} Å. The final structure was then overlaid with the averaged structure of all 211 frames.

*Determination of Conotoxin*AChBP Interaction Constants.* Second-order association and first-order dissociation rate constants (k_{on} and k_{off}) were determined by direct measurements of conotoxin binding to *Aplysia californica* acetylcholine binding protein (A-AChBP), as well as *Bulinus truncatus* acetylcholine binding protein. The stopped-flow technique was used to measure rates of quenching of intrinsic AChBP tryptophan fluorescence upon binding of the cono-

Table 1: Sequence Alignment of α-Conotoxins, ρ-Conotoxin, and χ-Conotoxins[a]

Name	Sequence	Globular m/n#	Ribbon m/n#	Species	Ref
4/(3-7) α-conotoxin					
EpI	GCCSDPRCNMNNPDYC*	5/12	13/4	*C. episcopatus*	(49)
PnIA	GCCSLPPCAANNPDYC*	5/12	13/4	*C. pennaceus*	(50)
PnIB	GCCSLPPCALSNPDYC*	5/12	13/4	*C. pennaceus*	(50)
MII	GCCSNPVCHLEHSNLC*	5/12	13/4	*C. magus*	(51)
EI	RDOCCYHPTCNMSNPQIC*	5/12	13/4	*C. ermineus*	(52)
AUIA	GCCSYPPCFATNSDYC*	5/12	13/4	*C. aulicus*	(8)
AUIC	GCCSYPPCFATNSGYC*	5/12	13/4	*C. aulicus*	(8)
GIC	GCCSHPACAGNNQHIC*	5/12	13/4	*C. geographus*	(53)
GID	IRDγCCSNPACRVNNOHVC	5/12	13/4	*C. geographus*	(19)
AnIB	GGCCSHPACAANNQDYC*	5/12	13/4	*C. anemone*	(47)
AUIB	GCCSYPPCFATNPD C*	5/11	12/4	*C. aulicus*	(8)
Vc1.1	GCCSDPRCNYDHEI C*	5/11	12/4	*C. victoriae*	(54)
ImI	GCCSDPRCAWR C*	5/8	9/4	*C. imperialis*	(27)
ImII	ACCSDRRCRWR C*	5/8	9/4	*C. imperialis*	(21)
BuIA	GCCSTPPCAVLY C*	5/9	10/4	*C. bullatus*	(55)
OmIA	GCCSHPACNVNNPHICG*	5/12	13/4	*C. omaria*	(56)
3/5 α-conotoxin					
MI	GRCCHPA CGKNYS C*	4/9	10/3	C. *magus*	(51)
GI	ECCNPA CGRHYS C*	4/9	10/3	C. *geographus*	(57)
GIA	ECCNPA CGRHYS CGK*	4/9	10/3	C. *geographus*	(57)
GII	ECCNPA CGKHFS C*	4/9	10/3	C. *geographus*	(57)
SI	ICCNPA CGPKYS C*	4/9	10/3	C. *striatus*	(58)
ρ conotoxin					
TIA	FNWRCCLIPACRRNHKKFC*	5/12	13/4	C. *tulipa*	(11)
χ conotoxin					
CMrVIA	VCCGYKLCHO C	5/7	8/4	C. *marmoreus*	(9;11)
CMrX	GICCGVSFCYO C	5/7	8/4	C. *marmoreus*	(9)
MrIA	NGVCCGYKLCHO C	5/7	8/4	C. *marmoreus*	(10;11)
MrIB	VGVCCGYKLCHO C	5/7	8/4	C. *marmoreus*	(11)

[a] Four conserved cysteine residues were used to align the sequences. α-Conotoxins are divided into the 4/(3−7) and 3/5 classes based on the intercysteine spacing. The conserved C-terminal amidation seen in all (except conotoxin GID) is represented by an asterisk (*). The native disulfide pairings are shown above each class of conotoxins. # (*m/n*) refers to the number of residues in the first and second intercysteine loops, respectively, when the peptides adopt either the globular or ribbon conformation upon formation of the two disulfide bridges.

toxins at micromolar concentrations. k_{on} and k_{off} were obtained by linear fit of first-order decay rates of AChBP fluorescence, at several conotoxin concentrations. The first-order dissociation constants were also determined by measurements of the rate of return of AChBP fluorescence in the stopped-flow apparatus upon mixing conotoxin*AChBP complex with 1000-fold excess of competing ligand, gallamine or epibatidine.

Dissociation constants (K_d) of conotoxin*AChBP complex were also determined from the conotoxin concentration dependence of the pseudo-first order association rate, of A-AChBP ligands gallamine or (5-dimethylamino-naphthalene-1-sulfon-amido-ethyl)-tri-methyl-ammonium. The measurements were performed in 0.1 M phosphate buffer, pH 7.0 at 22 °C on a SX.18 MV stopped-flow instrument (Applied Photophysics).

A scintillation proximity assay (SPA, Amersham Biosciences) adapted for use in a soluble radioligand binding assay was additionally used to determine K_d for conotoxin binding to A-AChBP. Increasing concentrations of conotoxins were incubated with (+)-epibatidine and 0.5 nM binding sites of AChBP. Radioactivity was measured on a Beckman LS 6500 liquid scintillation counter.

RESULTS

Identification of Potential Structural Determinants for Folding. Table 1 shows the sequence alignment of α-conotoxins and χ/λ-conotoxins. Despite the four conserved cysteine residues, α-conotoxins as well as ρ-conotoxin exhibit the globular conformation with C_{1-3}, C_{2-4} disulfide pairing while χ/λ-conotoxins adopt a ribbon conformation with C_{1-4}, C_{2-3} disulfide pairing. A systematic analysis of these sequences highlights the key differences between these two closely related families of conotoxins: (a) All α/ρ-conotoxins (except GID conotoxin (*19*)) are amidated at the C-terminal end. C-terminal amidation is not conserved in χ/λ-conotoxins; (b) Sequences of α-conotoxins contain at least one proline residue in the first intercysteine loop. A conserved proline is found in the penultimate position in the first intercysteine loop of both 4/ (*3*−*7*) and 3/5 classes of α-conotoxins. However, this kink-inducing residue is consistently absent from the first intercysteine loop of the four

Table 2: Folding Studies of Synthetic Peptide Variants in Oxidation Conditions[a]

Peptide	Sequence	Conformation in Folding Buffer			Conformation in Denaturing Buffer		
		Globular	*Ribbon*	*Beaded*	*Globular*	*Ribbon*	*Beaded*
ImI P6 Amide [12]	GCCSDPRCAWRC-CONH2	54.0±0.4 (52.1±0.1)	43.0±1.0 (43.8±0.3)	3.0±0.6 (4.0±0.2)	48.9±0.1 (48.3±0.2)	39.7±0.0 (38.0±0.4)	11.4±0.0 (13.7±0.1)
ImI P6 Acid [12]	GCCSDPRCAWRC-CO**OH**	30.1±0.6 (29.4±0.3)	67.2±0.4 (67.9±0.1)	2.7±0.5 (2.8±0.2)	37.6±0.7 (50.3±0.3)	44.6±1.8 (39.8±1.1)	17.8±2.4 (9.9±1.0)
ImI K6 Amide	GCCSD**K**RCAWRC-CONH2	30.2±1.5 (29.4±2.8)	68.5±1.7 (69.7±2.5)	1.3±0.4 (0.9±0.3)	41.5±1.9 (48.0±1.6)	56.8±1.7 (52.0±1.6)	1.7±1.0 (~0)
ImI K6 Acid	GCCSD**K**RCAWRC-CO**OH**	19.8±0.3 (20.1±0.8)	76.2±0.4 (74.4±1.1)	4.1±0.5 (5.5±0.4)	30.2±0.2 (30.3±1.5)	53.1±0.4 (49.9±3.1)	16.7±0.6 (19.9±1.8)
ImI A6 Amide	GCCSD**A**RCAWRC-CONH2	27.0±1.6 (24.6±0.3)	70.9±1.4 (72.4±0.5)	2.1±0.2 (3.1±0.3)	29.8±0.1 (31.1±1.2)	55.0±0.8 (54.3±1.1)	15.2±1.0 (14.6±0.2)
CMrVIA K6 Acid	VCCGYKLCHO C-COOH	31.3±0.9 (30.8±0.5)	52.9±0.3 (54.5±0.5)	15.8±0.5 (14.7±0.1)	35.6±0.9 (35.0±1.9)	53.6±0.7 (55.8±0.3)	10.9±0.2 (9.2±2.1)
CMrVIA K6 Amide	VCCGYKLCHO C-CO**NH2**	34.0±0.6 (36.2±1.7)	48.8±1.0 (46.8±2.6)	17.2±0.4 (17.0±0.9)	37.7±1.8 (29.7±1.6)	53.0±0.5 (60.3±1.9)	9.3±1.30 (10.0±0.3)
CMrVIA P6 Acid	VCCGY**P**LCHO C-COOH	82.9±0.4 (84.0±0.4)	3.5±0.3 (3.0±0.1)	13.6±0.4 (13.0±0.4)	85.6±0.8 (87.0±1.6)	7.1±0.2 (6.5±0.1)	7.3±0.7 (6.5±1.4)
CMrVIA P6 Amide	VCCGY**P**LCHO C-CO**NH2**	93.1±0.7 (93.3±0.4)	5.3±0.7 (5.4±0.3)	1.5±0.1 (1.3±0.1)	82.0±5.6 (88.6±2.2)	14.7±4.8 (8.3±1.5)	3.3±0.8 (3.1±0.8)

[a] Oxidation was conducted in both folding buffer as well as denaturing buffer. Predominant isoforms from oxidation of each variant were identified as globular or ribbon conformation as indicated by coelution on HPLC as well as 1D NMR experiments (Figure 2). The poorly favored beaded conformation was identified as the third chromatographic peak with the same mass. All oxidation studies were conducted in triplicate. Data in parenthesis represents results obtained from oxidation studies conducted using glutathione redox conditions.

currently known members of the χ/λ-conotoxins; and (c) χ/λ-conotoxins have only two residues in the intercysteine loop 2, with the second residue being a hydroxyproline. In contrast, the second intercysteine loop in α-conotoxins tends to be slightly longer. Further, when proline is present within the second loop of α-conotoxins, it is usually situated at a different position. We propose that these conserved structural features in these two families of conotoxins are responsible for the variation in folding tendencies and thereby, act as conformational switches. The C-terminal amidation and proline in the first intercysteine loop may help in inducing globular conformation, whereas the loop size of the second intercysteine loop may be useful in retaining the ribbon conformation. These observations laid the basis for design of the synthetic variants, in which the contributions of C-terminal amidation as well as the proline residue in the first intercysteine loop were sequentially examined. We chose ImI conotoxin as a model because it is the shortest and a widely studied α-conotoxin (*20*−*33*). Except for the conserved C-terminal amidation and disulfide linkages, no other post-translational modification was noted in ImI conotoxin. Unlike the 3/5 GI α-conotoxin examined earlier (*5*), the length and intercysteine loop sizes of the 4/3 ImI α-conotoxin also match those of the 4/2 χ/λ-conotoxins closely (Table 1).

Chemical Synthesis of Conotoxin Analogues. Earlier, we reported the influence of C-terminal amidation on the folding tendency of ImI conotoxin and its variants (*12*). To investigate the role of the conserved proline residue in the first intercysteine loop, ImI K6 Amide was prepared. In this variant, Pro-6 of ImI conotoxin was replaced with a lysine, commonly found in the same position of χ/λ-conotoxins sequences. Second, ImI K6 Acid provides an alteration in C-terminal amidation and first intercysteine loop proline in a single variant. Finally, proline was replaced with alanine in the ImI A6 Amide variant to examine the role of the imine residue while minimizing changes to the side chain.

To test the reciprocal conformational switch, we incorporated these structural features in synthetic analogues of CMrVIA χ/λ-conotoxins: CMrVIA K6 Acid represents the native sequence of CMrVIA conotoxin, while CMrVIA K6 Amide was synthesized to incorporate a C-terminal amide that is absent from the native sequence. Both amidated and free carboxylic acid analogues of CMrVIA P6 variants were also synthesized to examine the effect of substituting Lys-6 of CMrVIA conotoxin with a proline residue (Table 2).

We also synthesized regiospecific disulfide variants to the ImI and CMrVIA conotoxin analogues by two-step selective deprotection scheme. For each variant, both the globular and ribbon conformations were assembled. The beaded conformation was not examined due to a much lower tendency of forming disulfide bridges between the vicinal cysteine residues.

Folding Studies. The purified and reduced peptides were subjected to oxidation conditions by stirring in either glutathione redox system under nitrogen blanket for 4 h or in air for 48 h. They were then separated using analytical C18 HPLC column. Each of the synthetic variants folded into three monomeric isoforms upon oxidation, corresponding to the three peaks observed on the chromatograms (Figure 1, Supplementary Figure S2, Supporting Information). Each peak contained peptides that were completely oxidized as verified by reduction of four mass units, corresponding to the formation of two disulfide bridges (Supplementary Table

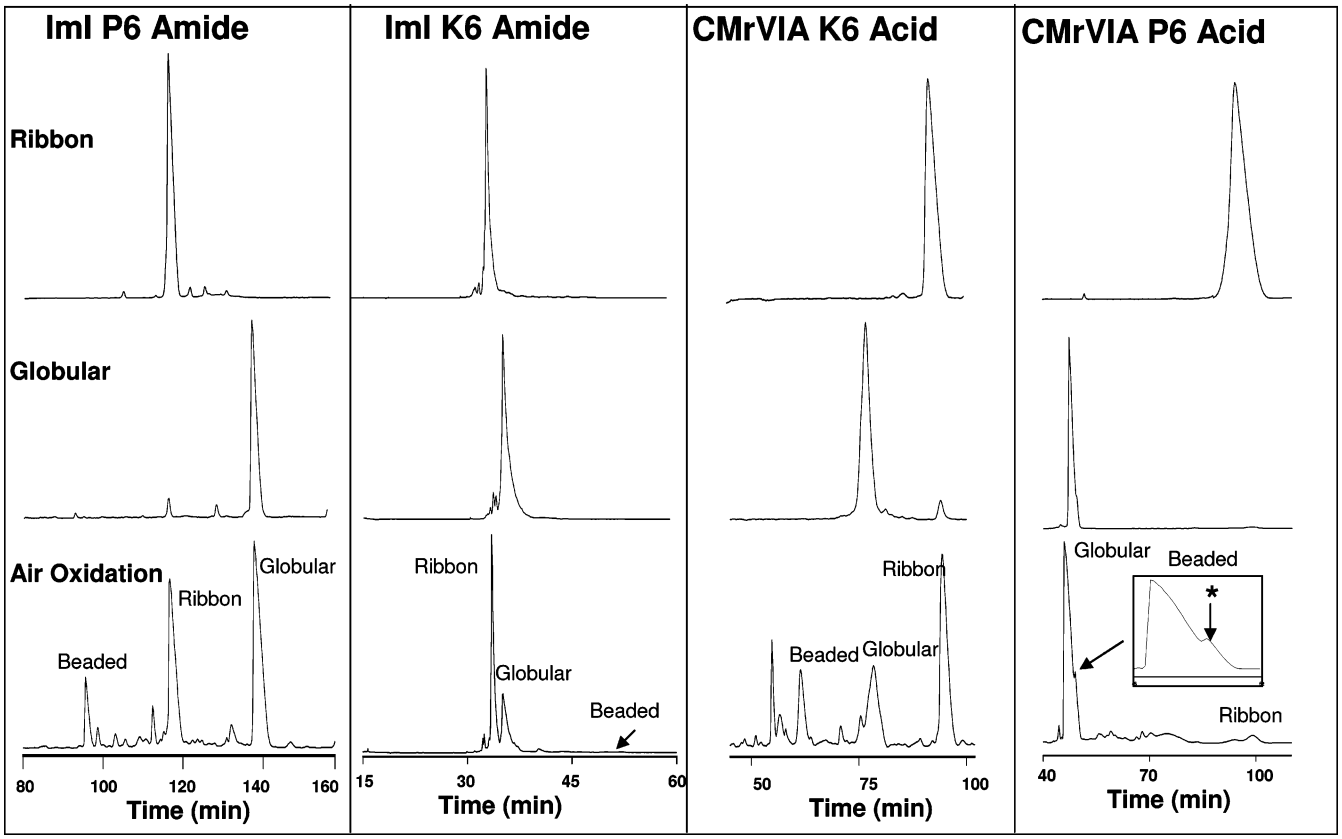

FIGURE 1: Chromatographic profiles of conotoxin analogues. Retention times of the regiospecifically synthesized conformation were compared and matched with the dominant isoform derived from air oxidation. Retention time of dominant peak 3 of ImI P6 Amide coincides with that of the regiospecifically synthesized globular conformation. Peak 1 of ImI K6 Amide and peak 3 of CMrVIA K6 Acid coelute with the ribbon conformation of the respective variants, and the substituted CMrVIA P6 Acid variant coelutes with the globular conformation.

1 and Figure S1, Supporting Information). Glutathione redox also generated isoforms in similar proportions, except for ImI P6 Acid in the denaturant buffer. The various structural isoforms were identified initially by comparing the retention times of the isoforms of oxidized conotoxin analogues with regiospecifically synthesized globular and ribbon conformations (Figure 1, Supplementary Figure S2, Supporting Information). The relative percentages of the three isoforms formed in the oxidation studies were determined by calculating the area under each peak (Table 2). The conformation of the dominant form for various peptides was also confirmed by NMR spectra and solution structure calculations (see below).

When allowed to fold, 54% of native ImI P6 Amide folds into the globular conformation (*12*). Substitution of the proline residue in the first intercysteine loop of ImI P6 Amide with a lysine residue caused ImI K6 Amide analogue to fold predominantly into the ribbon conformation, amounting to 68.5% of the total oxidized peptides. ImI A6 Amide variant was also synthesized and shown to have ~70% of the total oxidized peptide folding into the ribbon conformation. Substituting the C-terminal amide with a free carboxylic acid results in 67% of the ImI P6 Acid folding into the ribbon conformation (*12*). When both the C-terminal amidation and proline were replaced in the original sequence, ImI K6 Acid showed the greatest ribbon preference with 76% in that conformation. In all the cases, beaded conformations were disfavored (~1.2−4.1%). No significant differences in the folding tendencies were observed for the four ImI conotoxin analogues under glutathione redox compared to air oxidation conditions (Table 2). In addition to ImI K6 Amide variant, an ImI A6 Amide variant was also synthesized and shown to have ~70% of the total oxidized peptide folding into the ribbon conformation. Thus, the presence of proline residue in the first loop appears to act as a switch from ribbon to globular conformation. Replacement of this crucial imino acid residue with either the short aliphatic alanine, or the extended charged lysine, resulted in a switch of folding preference toward the ribbon form. C-Terminal amidation has an additive effect on the shift of folding tendencies serving to enhance the conformational switch. Thus, by two simple changes, the replacement of proline in the first loop and the removal of the C-terminal amide, the globular fold of the ImI conotoxin, an α-conotoxin was changed to the ribbon fold of a χ/λ-conotoxin.

To test whether a proline residue in the first loop and the C-terminal amide group would switch the ribbon fold of a χ/λ-conotoxin to globular fold of α-conotoxin, we performed reciprocal oxidation studies using CMrVIA χ/λ-conotoxin variants. This conotoxin possesses neither the proline in the first intercysteine loop nor the conserved C-terminal amidation. The native toxin exists in a ribbon conformation. As expected, native CMrVIA conotoxin (herein, described as CMrVIA K6 Acid) folds predominantly into the ribbon conformation (Table 2). Substitution of the lysine residue in the first intercysteine loop with a proline residue resulted in 83% of the oxidized peptides of CMrVIA P6 Acid variant to fold in the globular conformation. The CMrVIA P6 Amide analogue incorporates both the proline in the first intercysteine loop, as well as the C-terminal amidation. The

cumulative effect of the two structural features was apparent from the 93% globular isoform noted upon oxidation (Table 2). Thus, by these two simple changes, the ribbon fold of χ/λ-conotoxin was changed to globular fold in CMrVIA conotoxin.

Effect of Denaturant on Folding. In the presence of a guanidine hydrochloride, although major folding conformer of the ImI conotoxin analogues remained as the dominant isoform, there was a shift toward other conformers. However, the overall folding tendencies of the ImI conotoxin variants generally remained the same as when the peptides folded in nondenaturing, oxidizing conditions. For example, the beaded conformer, with its vicinal disulfide bridge (*34*−*43*), increased significantly (∼11.4−17.8%), except for ImI K6 Amide (1.7%). The most significant increase was noted for the ImI P6 acid and the ImI K6 acid. Thus, the presence of guanidine produced a greater distribution of isoforms in all four ImI variants (Table 2). These results indicate that side chain interactions promoted by H_2O contribute partially, but not fully, to the stable fold. The C-terminal Amide appears to resist the effect of denaturant and block the beaded conformation, particularly in the case of ImI K6 Amide, in which the beaded conformation was lowered from 16.7 to 1.7% (Table 2). In contrast, the presence of denaturant in the folding buffers did not seem to markedly influence the folding propensities of the CMrVIA conotoxin analogues. With the exception of CMrVIA P6 Amide, other variants show significant amounts of beaded conformers. The percentage of the unfavorable beaded conformation ironically was reduced in the presence of the denaturant buffer (Table 2). It is possible that the shorter and more restrained second intercysteine loop of CMrVIA conotoxin results in a difference in response to the denaturing folding environment when compared to the longer ImI conotoxin.

Significant differences were found in the folding tendencies when the peptides were folded under redox conditions in the presence of denaturants. In the case of ImI P6 acid, air oxidation conditions yielded 44.6 and 37.6% of peptides in ribbon and globular conformation, respectively. In contrast, under redox conditions, it yields 39.8 and 50.3% in ribbon and globular conformations, respectively (Table 2). ImI K6 acid, which lacks both the determinants required for folding in globular conformation, shows the most significant contribution of side chains for the folding, particularly in redox conditions. The ratios of beaded/globular/ribbon conformations were approximately 1:1.5:2.5. These ratios are expected to be closer to 1:1:1, if folding was determined completely by side chain interactions and 6 M guanidine hydrochloride was sufficient to completely abolish the contributions of all side chain interactions. Interestingly, ImI K6 Amide folds into ribbon and globular conformations with a ratio approaching 1:1. In this case, the beaded conformation is almost undetectable (Table 2). Thus, the C-terminal Amide in ImI K6 Amide completely blocks formation of beaded conformation. These results indicate that side chains play a crucial role in the folding of ImI K6 Amide, and the presence of guanidine hydrochloride abrogates these contributions leading to near equal proportions of globular and ribbon conformations.

NMR Studies of Conotoxin Variants. To confirm the folding conformations of the variants, we determined the solution structure of all the peptides in their most favored conformations. The Amide signals of one-dimensional (1D) NMR spectra for all the peptides were well-resolved, spanning the range of 7.5−9.2 ppm, indicative of well-ordered structures. Disulfide pairings of the dominant isoforms from the variants were identified by HPLC retention times and then verified by comparing the 1D proton NMR spectra with their corresponding regiospecifically synthesized peptides (Figure 2, Supplementary Figure S3, Supporting Information).

Temperatures yielding the highest resolution 1D NMR in the Amide region were chosen for the 2D proton NMR. Overall, the peptides yielded 2D NMR spectra of good quality from which sufficient distance constraints were obtained for structural modeling. In all cases, only a single set of associated spin-systems was observed, and no clear evidence for the presence of minor conformers was observed (Figure 3, Supplementary Figure S4, Supporting Information). Residues were assigned with TOCSY and ROESY spectra, using a sequential assignment strategy (*4*, *18*). All the variants showed distinct deviation of CαH chemical shift from the random coil values (*44*), indicating of stable secondary structure for each of the analogues (Figure 4, Supplementary Figure S5, Supporting Information).

ImI P6 Amide. TOCSY spectra and ROE connectivity diagrams for the dominant peak of ImI P6 Amide are shown in Figure 3A. The TOCSY spectrum obtained was similar in chemical shifts reported by Rogers et al. (*32*) for the native globular conformation of ImI α-conotoxin with the Amide region resolving in the range of 7.5−9.0 ppm and having an identical sequential assignment. A total of 88 ROEs were obtained from the ROESY spectra, of which 19 were inter-residue constraints, and 69 were intraresidue ROEs. Distance constraints obtained from ROESY spectrum fitted the earlier reported ImI conotoxin structure well, with only two deviations (less than 0.3 Å). Temperature coefficients as well as the $^3J_{NH}-C_{\alpha H}$ coupling constants derived (Figure 4A) from the spectra of ImI P6 Amide were also similar to those presented earlier (*32*). Supplemented with the HPLC coelution profiles, these data confirm that ImI P6 Amide peptide used as a reference for the folding studies, has the same conformation as the structure of the native protein deposited in Protein Data Bank (PDB ID 1IM1). Therefore, this structure was used for comparison.

ImI P6 Acid. ImI P6 Acid yielded 2D NMR spectra of good dispersion, from which 110 ROEs were obtained from the ROESY spectra (*12*), (Supplementary Figure S4, Supporting Information). Of these, 37 represented inter-residue ROEs and the remaining 73 were intraresidue ROEs. The presence of a strong αH-*δH* ROE between Asp-5−Pro-6 suggests a trans peptide bond between these two residues. Identification of the Cβ*H*−Cβ*H* ROEs between Cys-3−Cys-8 and Cys-2−Cys-12 is indicative of the disulfide pairing characteristic of the ribbon conformation. Temperature coefficients of Amide resonance for Ser-4, Asp-5, Arg-7, Cys-8, and Cys-12 were less negative than −4.0 ppb/ K. This suggests the presence of solvent shielding or intramolecular hydrogen bonded Amide for these residues (Supplementary Figure 5A, Supporting Information).

Even though ImI P6 Acid and ImI P6 Amide differ only by the C-terminal residue, the 2D spectra differences illustrate the nonidentity of secondary structure and microenvironment

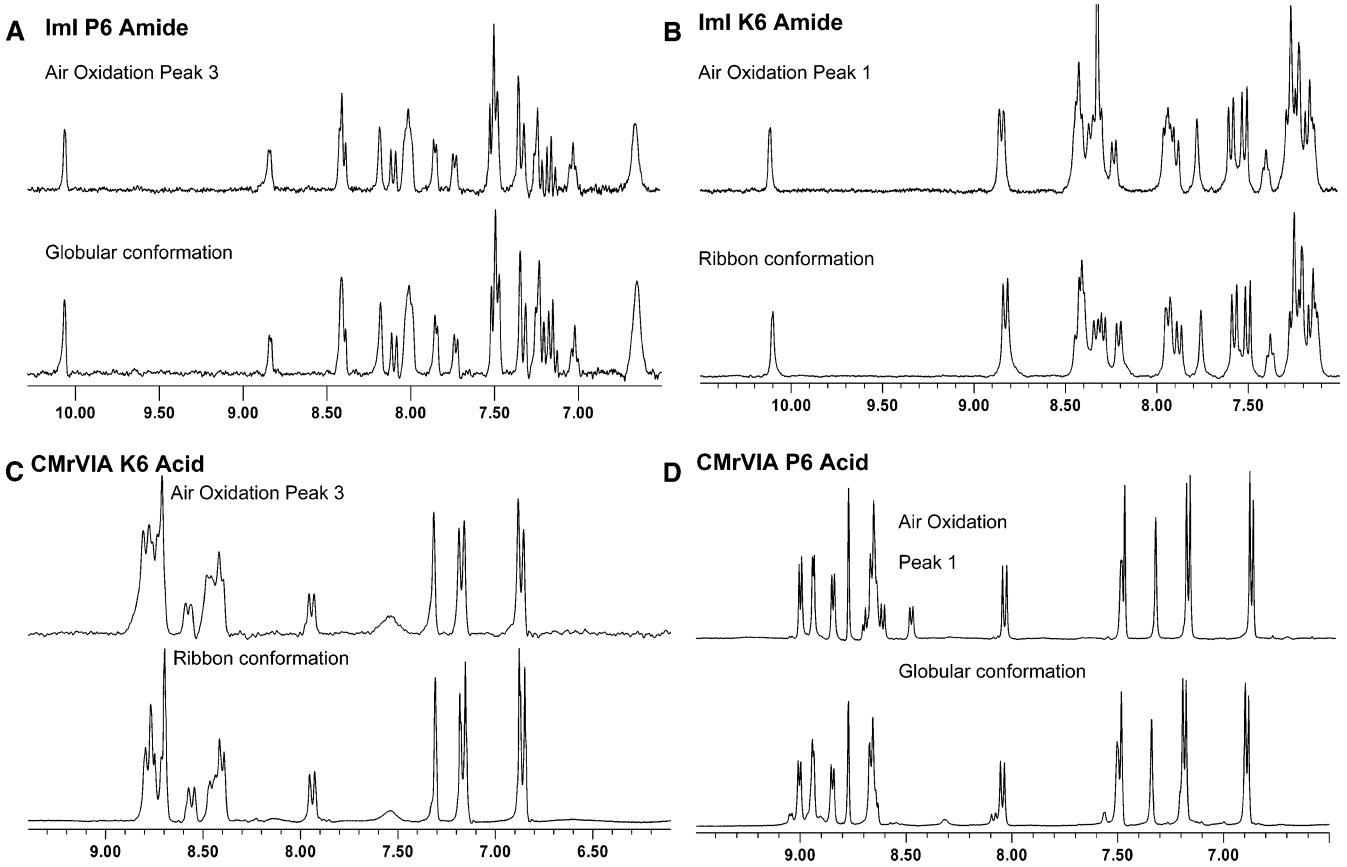

FIGURE 2: One-dimensional NMR analysis of dominant isoforms derived from oxidation studies. Products of oxidation studies were separated by HPLC and sequentially labeled as peak 1−3 according to sequence of elution. The 1D ^{1}H NMR spectra of (A) ImI P6 Amide peak 3 and (B) ImI K6 Amide peak 1 were compared with their respective ribbon conformations, (C) CMrVIA K6 Acid peak 3 with the corresponding globular conformation, and (D) CMrVIA P6 Acid peak 1 with its ribbon conformer.

for the two peptides (Supplementary Figure S5, Supporting Information) (*12*).

ImI K6 Amide and ImI K6 Acid. A total of 32 inter-residue ROEs and 72 intraresidue ROEs were obtained for ImI K6 Amide, while 40 inter-residue ROEs and 76 intraresidue ROEs were observed for ImI K6 Acid (Figure 3B and Supplementary Figure S4, Supporting Information). The presence of the CβH−CβH ROE between Cys-3−Cys-8 for the ImI K6 Amide indicates that the disulfide pairing is analogous to that seen in ribbon conformation. CβH−CβH interactions between the cysteine residues of the ImI K6 Acid could not be resolved due to overlapping ROEs.

Nearly all the residues in both the peptides were solvent exposed, with the exception of Cys-2, Asp-5, Arg-7, and Cys-8 residues, which had temperature coefficients that suggested solvent shielding. $^3J_{NH}-C_{\alpha H}$ coupling constants derived from both spectra indicated values of less than 5 Hz for residues Lys-6 and Ala-9. All other residues presented values which fell in the range of 5−8 Hz. The numerous $d_{NN(i,i+1)}$ connectivities suggest that both structures are likely to contain several turns throughout the sequence, especially for residues located between Lys-6 and Arg-11 (Figure 4B and Supplementary Figure S5C, Supporting Information). TOCSY amide region resonances for the two spectra were also fairly similar, with Cys-8 and Asp-5 shifting upfield, and Arg-7 shifting downfield of ImI K6 Amide. All variations in chemical shifts in the amide region were within ~0.3 ppm between the two spectra. As with ImI P6 Acid that is also held in the ribbon conformation, the Cβ protons of Cys-3, Asp-5, and Cys-8 were poorly resolved, indicative of less well-defined side chain orientation for these residues in the ribbon isoform.

Unlike ImI P6 Acid and ImI P6 Amide, both ImI K6 Acid and ImI K6 Amide presented similar 2D spectra, temperature coefficient patterns, $^3J_{NH}-C_{\alpha H}$ coupling constants, as well as the chemical shift index for CαH (Figure 4F). Comparisons of the 2D TOCSY spectra for the two ImI K6 variants with the ImI P6 Acid also reveal similarity for the amide chemical shifts of the various spin systems. This indicates a marked structural resemblance between ImI K6 Acid and ImI K6 Amide, and to an extent, ImI *P*6 Acid.

ImI A6 Amide. The 2D NMR spectra for the dominant isoform of ImI A6 amide had a reasonable dispersion of amide signals (Supplementary Figure S4, Supporting Information). A total of 107 ROEs were unambiguously assigned. Of which, 70 were intraresidue ROEs, and the remaining 37 were inter-residue ROES. The CβH−CβH ROEs of the cysteine residues involved in the disulfide bridge formation could not be resolved due to the overlapping signals. Asp-5, Arg-7, and Cys-8 presented a temperature coefficient that is less negative than −4.0 ppb/ K, indicative of solvent shielding of these residues (Supplementary Figure S5, Supporting Information).

The chemical shifts for the various spin systems relate well with those of ImI P6 Acid variant, as both show close sequence identity, and oxidize to the ribbon conformation as the final conformation. The chemical shift indexes for the two peptides were also generally similar, with positive

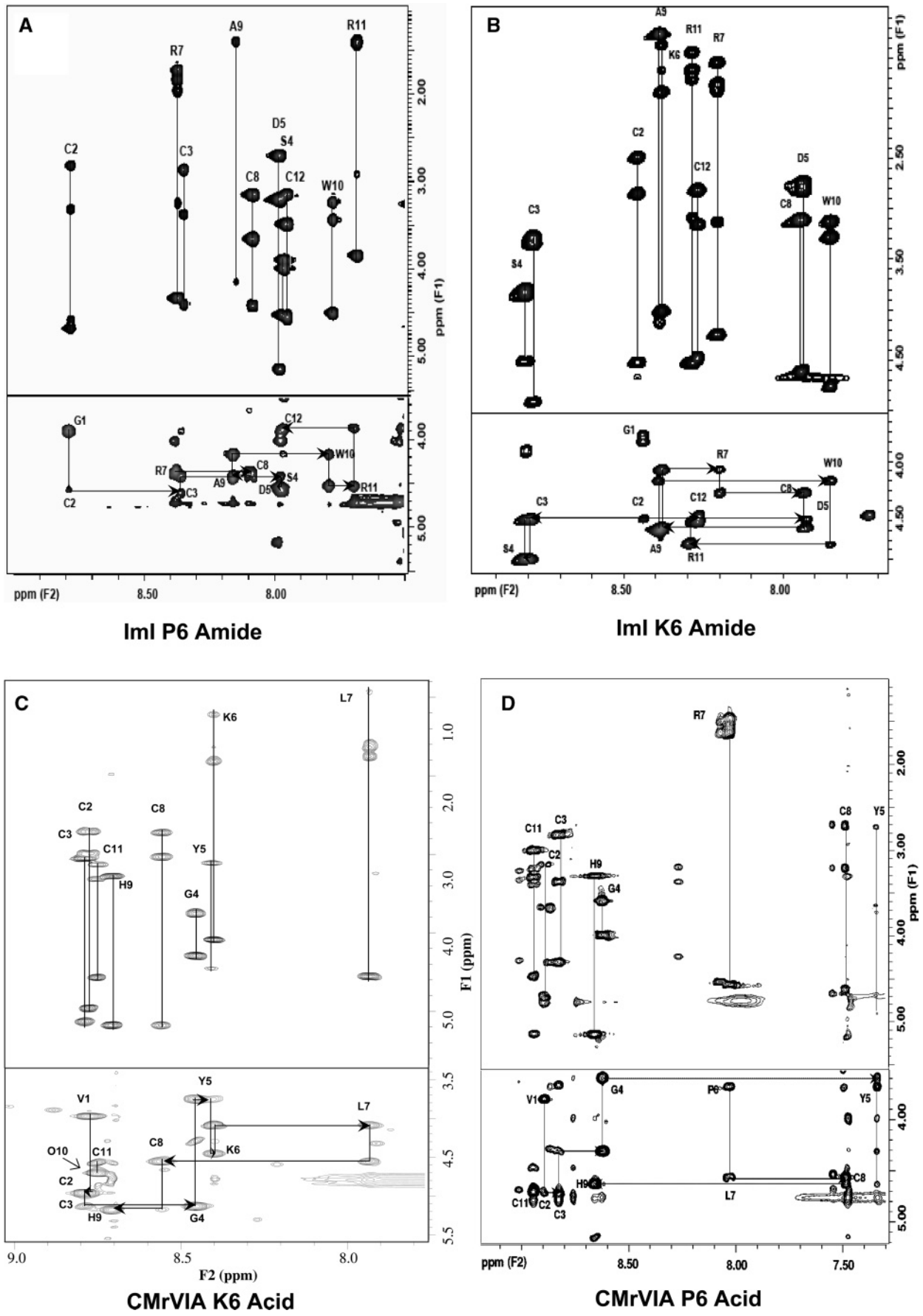

FIGURE 3: Two-dimensional NMR spectra and sequential assignments. The diagrams comprising of 70 ms TOCSY αH−NH region (top panel) and 300 ms ROESY region (bottom panel). 2D NMR experiments were carried out on samples dissolved in 90% H_2O and 10% D_2O, pH 3.1 on Brüker DRX-500 MHz spectrometer. Experiments for (A) ImI P6 Amide peak 3, (B) ImI K6 Amide peak 1, (C) CMrVIA K6 Acid peak 3, and (D) CMrVIA P6 Acid peak 1 were carried out at 298, 300, 300, and 303 K, respectively.

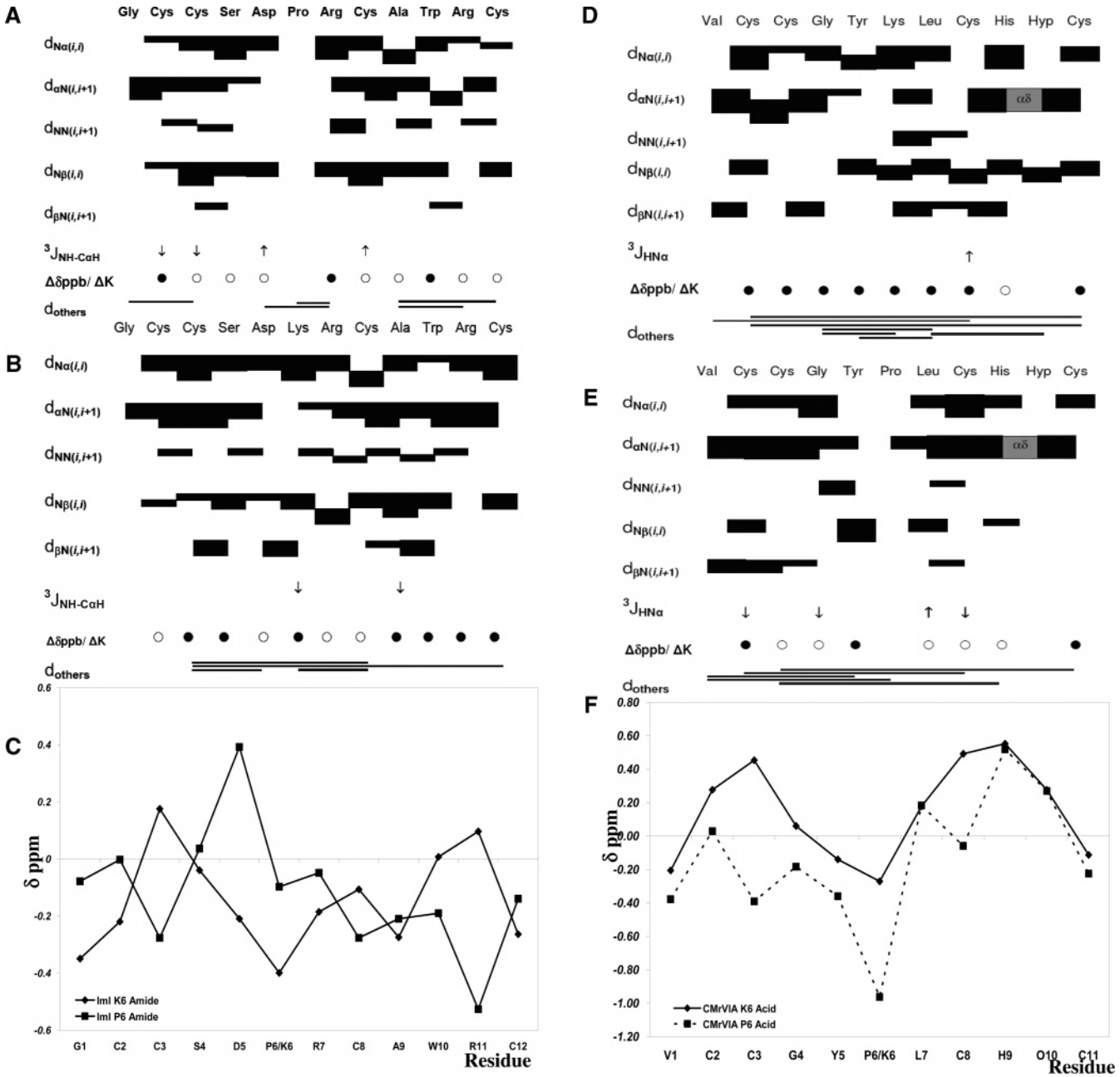

FIGURE 4: Summary of 2D NMR data. Panels (A) and (B) show details on the sequential ROE data, $^3J_{NH-C\alpha H}$ coupling constants, temperature dependence of amide chemical shifts, as well as medium- and long-range ROEs for ImI P6 Amide and ImI K6 Amide, respectively. NMR data for CMrVIA K6 Acid and CMrVIA P6 Acid are similarly summarized in panels (D) and (E). The thickness of the bars represents the relative intensity of the ROEs as depicted in the 2D ROESY spectra (weak, medium, and strong). ↑ and ↓ represent $^3J_{NH-C\alpha H}$ coupling constants above 8.5 Hz and below 5.0 Hz, respectively. ○ represents temperature coefficient of amide chemical shifts > −4.0 ppb/K, and ● represents temperature coefficients < −4.0 ppb/K. ROE between Asp-5 CαH and Pro-6 CδH is indicated in the diagram as a gray shaded box. Overlapping ROE of an ambiguous assignment is marked with (*). Panels (C) and (F) compare the deviation of experimental Cα protons chemical shift values from random coil chemical shift values for the respective amino acids in both ImI P6 Amide and ImI K6 Amide, as well as CMrVIA K6 Acid and CMrVIA P6 Acid, respectively. ROE lines presented under d_{others} refer to the miscellaneous ROEs between any protons of the residues at the two ends of the lines.

deviation from random coil values between the segments of Cys-3 to Asp-5, and Trp-10 to Arg-11. However, the spectrum is distinctly different from that observed for ImI P6 Amide despite their greater resemblance in sequence. The chemical shifts for Cys-2, Cys-3, Ser-4, Ala-9, Trp-10, and Arg-11 are similar to those noted in ImI P6 Acid's spectra. Spin systems that exhibited minor changes in chemical shifts included Asp-5 and Cys-8, which fell within 0.2 ppm from the values noted in the spectrum of ImI P6 Acid. Arg-7's chemical shift was noted to have moved up field by 0.3 ppm, likely to be a result of the difference in the position 6 residue in the two peptides. Cys-12 was noted to have 0.3 ppm downfield shift as compared to the same residue seen in ImI P6 acid. This shift is likely to be a result of the difference between variants in C-terminal functional group.

CMrVIA K6 Acid and CMrVIA K6 Amide. 2D NMR spectra of CMrVIA K6 Acid and CMrVIA K6 Amide are presented in Figure 3C and Supplementary Figure S4, respectively. Of the total of 91 ROEs obtained from the spectra of CMrVIA K6 Acid, 60 were intraresidue, and the

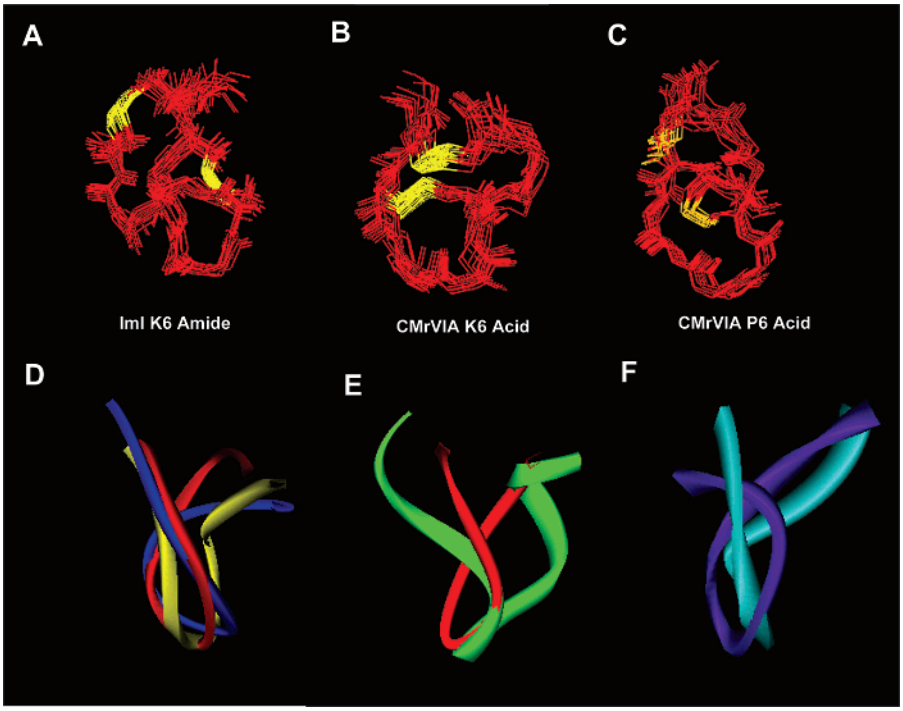

FIGURE 5: Backbone superposition of calculated structures for dominant isoforms of conotoxin analogues. (A) ImI K6 Amide, (B) CMrVIA K6 Acid, and (C) CMrVIA P6 Acid. Families of 15 lowest energy structures are overlaid with the averaged calculated structure. Sulfur atoms and the corresponding disulfide bridges of the structures are highlighted in yellow. (D) Superposition of the ribbon forms for ImI P6 Acid (red), ImI K6 Acid (yellow), and ImI K6 Amide (blue). rmsd for the ribbon forms of the different analogues ranged from 2.07 to 2.18 Å. (E) Backbone superimposition of ImI P6 Amide (green) with ImI P6 Acid (red) gave a rmsd of 3.5 Å, while (F) superimposition of CMrVIA K6 Acid (magenta) and CMrVIA P6 Acid (cyan) gave an rmsd of 2.35 Å.

remaining 31 ROEs were inter-residue ROEs (*45*). Fifty-two of the 86 ROEs identified for CMrVIA K6 Amide were intraresidue ROEs, and the remaining 34 were inter-residue ROEs. αH−δH ROEs were identified between residue His-9 and Hyp-10 for both peptides, which suggest a trans peptide bond between these two residues. The ROEs between Cys-2 βH to Cys-11 βH seen in both variants verify the C_{1-4}, C_{2-3} disulfide connectivity characteristic of the ribbon conformation.

In CMrVIA K6 Acid, in contrast, only Gly-4, Lys-6, Cys-8, and His-9 of CMrVIA K6 Amide were solvent shielded. Positive deviations of αH chemical shift index were observed for the regions between Cys-2−Gly-4 and Leu-7−Hyp-10 of CMrVIA K6 Acid variant, and Leu-7−Hyp-10 of the amidated analogue (Figure 4, Supplementary Figure S5, Supporting Information).

The spin systems of both amidated and non-amidated analogues of CMrVIA K6 variants presented with similar amide chemical shifts, with the exception of Tyr-5 and Cys-11, which were shifted within 0.2−0.3 ppm of the two spectra.

CMrVIA P6 Acid and CMrVIA P6 Amide. CMrVIA P6 Acid and CMrVIA P6 Amide yielded spectra that were very similar to one another (Figure 3, Supplementary Figure S4, Supporting Information). Almost all of the eight spin systems visible in the fingerprint region had similar amide chemical shifts, with the exception of Cys-11 residue, which had an upfield shift of 0.3 ppm in the amidated analogue. Chemical shift indices of CαH were also very similar to one another, with a positive deviation in the Cys-2−Gly-4, and Arg-7−Hyp-10 in both peptides. Solvent shielding was noted for most residues of both peptides, except Cys-2, Tyr-5, and Cys-11 in CMrVIA P6 Acid, and Cys-2, Gly-4, and Cys-11 in the amidated analogue (Figure 4, Supplementary Figure S5, Supporting Information).

Structural Determination. Molecular dynamics simulation for the dominant isoform of the various analogues was performed using the distance restraints derived from the ROE volumes of the ROESY spectra. Average conformations were derived from the 211 structures generated from trajectory analysis, and families of 15 final structures with the lowest energies were chosen to represent the solution structure for the peptides (Figure 5A−C, Supplementary Figure S6, Supporting Information). Figure 6 illustrates the overall conformation and electrostatic surfaces for calculated solution structure of the various peptides.

The calculated structure for ImI P6 Acid (PDB ID 2IGU) (*12*) exhibits a β-turn at Asp-5-Pro-6-Arg-7-Cys-8, owing to the disulfide bridge formed between Cys-3 and Cys-8 and the disulfide bridge between Cys-2 and Cys-12. The structure is further reinforced by hydrogen bonds between Asp-5 carbonyl group and Cys-8 amide proton, as well as Ser-4 amide with the carbonyl group of C-terminal carboxylic acid. These intramolecular hydrogen bonds observed in the resultant structure are consistent with the low-temperature coefficient chemical shifts of Ser-4 and Cys-8 amide protons.

As with the ribbon conformation of ImI P6 Acid, ImI K6 Acid (PDB ID 2IFJ) and ImI K6 amide (PDB ID 2IFZ) also possess a β-turn at Asp-5-Lys-6-Arg-7-Cys-8 and Lys-6-Arg-7-Cys-8-Ala-9, respectively. This was supported by the low $^3J_{NH}-C_{\alpha H}$ coupling constants of <5 Hz for Lys-6 in both variants. The numerous $d_{NN(i,i+1)}$ and $d_{N\alpha(i,i+1)}$ connectivities observed in the region of Gly-1−Asp-5 and Arg-7−Arg-11

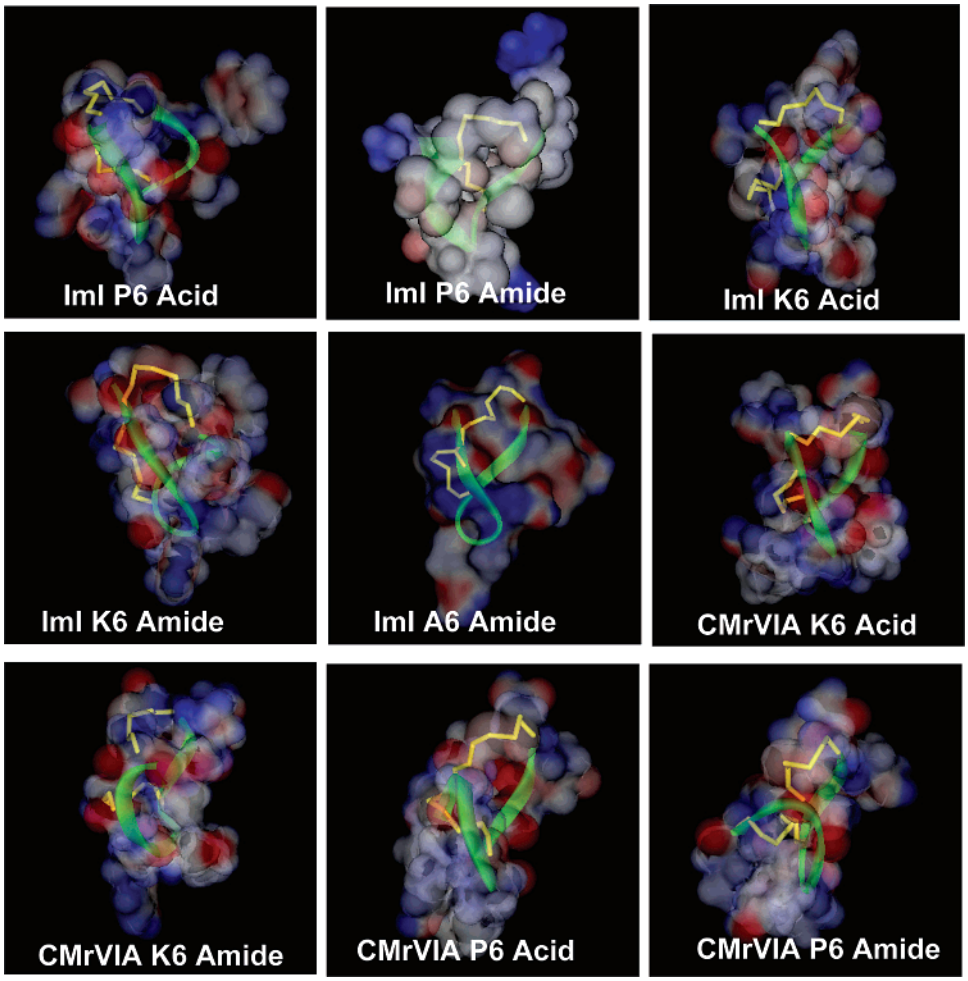

FIGURE 6: Electrostatic surface of solution structures for the dominant isoforms of conotoxin analogues. Solvent accessible surfaces of the respective variants are presented in similar orientations. Positive residues are highlighted in blue, while negatively charged residues are in red. Three-dimensional solution structure of ImI P6 Amide was obtained from Protein Data Bank (PDB ID 1IM1).

in the ROESY spectra are suggestive of an extended β-sheet structure. However, this secondary structural element was not noted in the final calculated structure, as with the case for most peptides of such small size. As such, these connectivities are indicative of a stable and defined structure around this segment of the peptide. This is in agreement with the positive chemical shift index of the αH around the same regions (Figure 4B, Supplementary Figure S5C, Supporting Information). The turn in ImI K6 Acid is further reinforced with a bifurcated hydrogen bond between Asp5 carbonyl with Arg-7 and Cys-8 amide protons. In ImI K6 Amide, hydrogen bonds are observed between Asp-5 Amide and Cys-3 carbonyl group, as well as between Arg-7 Amide proton with its own side chain amine proton. These hydrogen bonds are consistent with solvent shielding predicted from the temperature coefficient chemical shifts of amide protons (Figure 4).

Native CMrVIA K6 Acid sequence (PDB ID 2B5P) was identified to fold in the ribbon conformation, possessing β-turns as the predominant secondary structural element. The overall conformation is dictated by the disulfide bridge between Cys-3−Cys-8, forming a loose turn within the nonhelical pentapeptide region. The C-terminus of the molecule is tethered close to the N-terminus as a consequence of the restraining Cys-2−Cys-11 disulfide linkage. 2D NMR data of the CMrVIA K6 Amide analogue presented are largely similar to that of the native CMrVIA K6 Acid variant, with a calculated solution structure (PDB ID 2IHA) resembling the latter structure. However, an additional hydrogen bond was noted between amide proton of Gly-4 with the sulfur atom of Cys-3 residue in the native structure (*45*).

CMrVIA P6 Acid (PDB ID 2IH6) and CMrVIA P6 amide (PDB ID 2IH7) exhibit globular conformations. Both variants exhibit similar 2D NMR spectra and, consequently, the calculated solution structures. β-Turns were noted in regions between Val-1−Gly-4 and Tyr-5−Cys-8. These turns are maintained by the disulfide bridges formed between Cys-2−Cys-8 and Cys-3−Cys-11. The globular conformation is reinforced by a bifurcated hydrogen bond between the amide proton of Cys-8 with the carbonyl groups of Tyr-5 and Leu-7.

Analysis of the ϕ and ψ angles for the completed structures revealed that none of the residues for the various peptides lies in the disallowed region, while very few ($\leq$12.5%) reside in the generously allowed region of the Ramachandran plot (Table 3).

Structural Comparisons. The averaged structures of all ImI variants in ribbon conformation were overlaid, and the backbone rmsd values were measured. Despite the variation in amino acid sequence and C-terminal modification, all three ribbon forms overlaid to give a backbone rmsd of 2.07−2.18 Å (Table 4), suggesting similarity in overall backbone

Table 3: Structural Statistics for Calculated Conotoxin Structures

	ImI P6 Acid	ImI K6 Acid	ImI K6 Amide	ImI A6 Amide	CMrVIA K6 Amide	CMrVIA K6 Acid	CMrVIA P6 Amide	CMrVIA P6 Acid
Ramachandran Plot Analysis								
% in favored	30.0	30.0	54.5	81.8	75.0	45.5	50.0	37.5
% in additionally allowed region	60.0	70.0	36.4	9.1	25.0	54.5	37.5	50.0
% in generously allowed region	10.0	0.0	9.1	9.1	0.0	0.0	12.5	12.5
Atomic Root-Mean-Square with Mean Structure								
all atom rmsd	0.83 ± 0.13	0.81 ± 0.16	0.89 ± 0.11	1.08 ± 0.30	0.84 ± 0.12	0.78 ± 0.18	0.53 ± 0.15	0.55 ± 0.10
heavy atoms rmsd	0.70 ± 0.14	0.71 ± 0.16	0.72 ± 0.10	0.99 ± 0.30	0.71 ± 0.10	0.63 ± 0.10	0.44 ± 0.11	0.50 ± 0.11
backbone rmsd	0.48 ± 0.10	0.49 ± 0.12	0.44 ± 0.10	0.93 ± 0.33	0.54 ± 0.10	0.52 ± 0.10	0.35 ± 0.10	0.48 ± 0.10
Distance Constraints Violations								
violations > 0.3 Å	1	1	1	2	2	0	1	2
violations > 0.5 Å	1	0	1	0	1	2	4	3
Number of Constraints								
intraresidue	65	76	72	70	52	60	58	61
short range ($\|i - j\| = 1$)	23	26	29	33	29	20	31	46
medium range ($1 < i \leq 2$)	4	7	3	3	2	4	0	5
long range ($i > 2$)	7	7	2	1	3	7	9	11
total number	99	116	104	107	86	91	98	123

Table 4: Backbone rmsd Values of Overlaid Structures

	ImI K6 Acid	ImI K6 Amide	ImI P6 Acid
ImI P6 Amide	2.53	3.11	3.51
ImI P6 Acid	2.18	2.08	
ImI K6 amide	2.12		

structure (Figure 5D). ImI P6 Amide was also overlaid with its corresponding deamidated ImI P6 Acid (Figure 5E). The rmsd of over 3.5 Å between the native ImI conotoxin and its deamidated variant substantiates the difference in their secondary structures. The calculated 3D structure of ImI P6 Amide peptide presented a typical "globular" conformation seen in α-conotoxins instead of the flat conformation seen in the three ribbon forms. Pairwise backbone overlay of the native ribbon CMrVIA K6 Acid and the globular CMrVIA P6 Acid gave a rmsd of 2.35 Å.

Binding Assays with AChBP. To determine binding affinities of the various synthetic analogues of ImI conotoxin, the regiospecifically synthesized variants were examined in binding assays with *Aplysia californica* acetylcholine binding protein (A-AChBP) and *Bulinus truncatus* acetylcholine binding protein (B-AChBP). Chromatographic peaks identified as the beaded conformation were also subjected to the assay after estimation of peptide concentration by UV spectroscopy.

Dissociation constants for the interactions were determined by (a) intrinsic tryptophan fluorescence quenching of A-AChBP upon complex formation, (b) AChBP−conotoxin complex formation inhibiting the initial rates of association of either gallamine or (5-dimethylamino-naphthalene-1-sulfon-amido-ethyl)-tri-methyl-ammonium with A-AChBP, or (c) equilibrium competition of peptide with radiolabeled epibatidine or α-bungarotoxin to A-AChBP. Equilibrium competitions using the radiolabeled probes were also performed to compare the binding affinity of the ImI conotoxin analogues to both B-AChBP and A-AChBP (Figure 7).

Overall, modifications of the structural features that result in the disruption of the backbone conformation result in loss of conotoxin binding affinity. The loss of affinity can be roughly correlated with the extent of structural modifications from the ImI conotoxin template (Table 5). For example, ImI P6 Acid and ImI A6 Amide (PDB ID 2IFI) variants, which preserve the globular conformation, have K_d's within 200-fold of the wild type ImI conotoxin. ImI K6 Acid ribbon isoform, with the largest divergence of key features including the conformational-restraining proline residue, C-terminal amidation, and nonglobular conformation presented with the lowest binding affinity (K_d > 500 μM).

Substitution of the conserved C-terminal amide of ImI conotoxin with a free carboxylic acid resulted in a 3-fold reduction in the binding affinity of its globular conformation as compared to the wild type globular ImI conotoxin. The ribbon conformation of the same deamidated ImI P6 variant exhibited a binding affinity that is reduced a further 60-fold. Replacement of proline with a lysine in the sixth position of the sequence had a detrimental effect on binding affinity. The loss of affinity cannot be accounted for by the backbone conformation of the variants, as the ImI A6 Amide globular conformation, had a lower K_d of 150 nM compared to globular isoform of ImI K6 Amide with a K_d of 4.5 μM. The most likely contributing factor would be the steric electrostatic repulsion between the long polar side chain of lysine and the receptor pocket. However, the ImI A6 Amide globular conformation has a binding affinity that is still 100-fold lower than the wild type ImI conotoxin, indicating the importance of the backbone structure of the native globular conformation. When replacement of Pro-6 was combined with other structural modifications, the cumulative reduction in binding affinity was 3 orders of magnitude.

Kinetics of conotoxin ImI interaction with A-AChBP appears to be sensitive to any deviation from its native structure. The more sensitive dissociation rate constants were increased by 4 orders of magnitude or more for the weakest binding variants, while association rate constants were reduced by only 2−3-fold. Exceptions were the two weakest binding ImI P6 variants where both dissociation and association rate constants were reduced by about 1 order of magnitude.

A surprising finding noted from the binding assay is that although the beaded conformation is the thermodynamically least favored and rarely found in native proteins, its binding affinity to A-AChBP is still significant and does not appear to be the weakest among the folds.

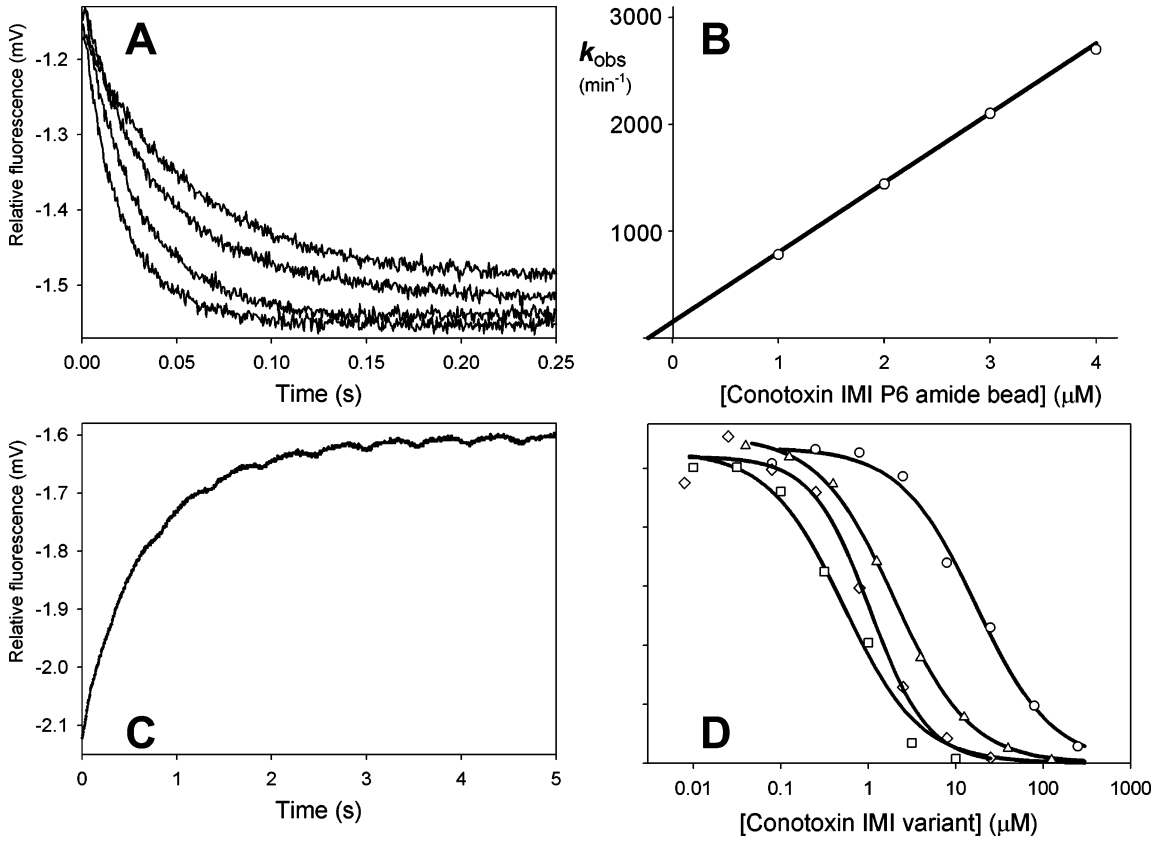

FIGURE 7: Determination of kinetic and equilibrium interaction constants of conotoxin ImI variants and A-AChBP. (A) Stopped-flow traces of intrinsic A-AChBP tryptophan fluorescence quenching as a function of time and conotoxin ImI P6 Amide bead concentration (1.0, 2.0, 3.0, and 4.0 uM). (B) The first-order rate constants of fluorescence quenching (k_{obs}) from panel A are plotted as a function of conotoxin concentration. The slope of the line yielded the second order association rate constant (k_{on}). (C) Determination of the first-order dissociation rate constant (k_{off}) for conotoxin ImI P6 Amide bead. Enhancement of the A-AChBP intrinsic tryptophan fluorescence upon the rate-limiting dissociation of conotoxin and immediate formation of A-AChBP*gallamine complex. (D) Radioactive competition assay for determination of K_d for conotoxin ImI variants: P6 Acid bead (squares), P6 Amide ribbon (diamond), P6 Amide bead (triangles) and K6 Amide globular (circles). Experimental points in panels B and D are determined as quadruplicate measurements. Panels A and C show single experimental traces.

Table 5: Kinetic and Equilibrium Constants for Interaction of Conotoxin ImI Variants with A-AchBP[a]

	K_d (nM)			k_{on} (10^8 M^{-1} min^{-1})	k_{off} (min^{-1})
	competition experiments		k_{off} /k_{on}		
conotoxin ImI	*B-AChBP*	*A-AChBP*	*A-AChBP*	*A-AChBP*	*A-AChBP*
P6 Amide globular (wt)	6.6	2.8	0.88[b]	10[b]	0.60[b]
P6 Acid globular	6.5	2.3	2.7	2.6	0.72
P6 Acid ribbon	95	48	170	3.0	51
P6 Acid bead	n.d.	140	460	0.57	25
P6 Amide ribbon	100	110	420	0.91	38
P6 Amide bead	220	220	240	6.1	150
A6 Amide globular	260	190	140	5.3	74
A6 Amide ribbon	>10 000	28 000	n.d.[c]	n.d.	n.d.
A6 Amide bead	>10 000	>10 000	n.d.	n.d.	n.d.
K6 Amide globular	>10 000	4700	n.d.	n.d.	5100
K6 Amide ribbon	>10 000	94 000	n.d.	n.d.	n.d.
K6 Acid ribbon	>10 000	>500 000	n.d.	n.d.	n.d.

[a] The equilibrium dissociation constant (K_d) is a mean of three to six experiments including radioactive probe and fluorescent probe competition experiments, as well as kinetic fluorescence experiments where it was calculated as a ratio of k_{off} and k_{on} rate constants. The association and dissociation rate constants (k_{on} and k_{off}) are mean of three to four experiments, and were determined from the rates of quenching of intrinsic A-AchBP fluorescence upon conotoxin binding. [b] From Hansen et. al (*24*). [c] n.d. = not determined.

DISCUSSION

α-Conotoxins and χ/λ-conotoxins are unique classes of compact peptide toxins isolated from *Conus* venoms. These peptides of 11−19 residues share four conserved cysteine residues. However, the disulfide pattern and their folding are distinctly different. α-Conotoxins have a globular conformation and C_{1-3}, C_{2-4} disulfide pairing. On the basis of the number of residues in the intercysteine loops 1 and 2, this family of toxins can be classified into the 4/(3−7) and 3/5 subfamilies, respectively (*2*). Despite the structural variations, they act as competitive inhibitors of nAChRs (*2*). On the other hand, χ/λ-conotoxins have a ribbon conforma-

tion and C_{1-4}, C_{2-3} disulfide pairing. So far, only four members of this family have been isolated, and they have four and two residues in the intercysteine loops 1 and 2, respectively (*9*−*11*). Unlike α-conotoxins, they block norepinephrine transporter (*11*). In both cases, non-native conformations are biologically less active (*4*, *9*), supporting the importance of the respective disulfide pairing and folding.

Earlier work by Zhang and Snyder (*5*) have added significant clarity to the involvement of amino acid residues and intercysteine spacing of α-conotoxins to their folding tendencies. However, the conotoxins studied were significantly different in intercysteine loops sizes from those in χ/λ-conotoxins. Recently, Buczek et al. demonstrated that the propeptide sequence did not influence the kinetics and thermodynamics of folding in GI α-conotoxin (*46*). Similarly, the propeptide sequence was not shown to have a substantial influence on the in vitro folding of ω-conotoxin MVIIA, an unrelated class of conopeptides (*34*). These studies suggest that information necessary for governing folding peptides is likely to be encrypted in the amino acid sequence of the mature conopeptides.

By comparing the amino acid sequences of α-conotoxins and χ/λ-conotoxins, we identified the contributions of the C-terminal amidation (*12*). In this work, we show that substitution of the critical proline residue of ImI P6 amide with a lysine residue in ImI K6 Amide favors the formation of the ribbon conformation (Table 2). This suggests that substitution of the kink-inducing proline residue with a bulky, charged side chain such as lysine does not favor formation of native globular conformation. Through the study of ImI A6 Amide, we have also demonstrated the importance of the conformationally restraining characteristics of proline in defining the conformation for folding and activity of the peptide toxin. When both the determinants are substituted in ImI K6 Acid, more than 76% folds into the ribbon conformation (Table 2). These results strongly suggest that the C-terminal amidation and the penultimate proline residue in the first intercysteine loop play important roles as conformational switches: when they are present the peptides fold in a globular conformation, and in their absence, peptides fold into the ribbon conformation. By reciprocally incorporating these structural features into CMrVIA χ/λ-conotoxin, the folding tendencies have shifted from a native ribbon-forming conotoxin framework to the non-native globular conformation.

Proline's side chain is fused with the main chain forming a pyrrolidine ring. The unusual amino acid chemistry allows proline to have both cis and trans peptide bonds. In addition, it always produces kinks or corners. Introduction of proline in the first intercysteine loop may induce a bend in the main chain of the peptide. Proline's capacity to introduce bends in the main chain could act as a conformational switch in conotoxins.

Under the various folding conditions, either the ribbon or the globular conformation is dominant. The beaded conformation is not preferred. In our in vitro folding studies, none of the four peptides folded 100% into a single conformation. Earlier folding studies conducted using organic solvents have also shown that the peptides fold in the native globular conformation as the predominant isoform (*5*, *19*, *27*, *47*). However, in vivo these peptides fold into a single conformation.

From the analysis of the folding tendencies of ImI P6 Amide and its analogues, the results for ImI K6 Acid suggest that in the absence of strong influencing factors such as proline residue in intercysteine loop 1 or neutralization of charge on the C-terminal by amidation there is a high tendency for the peptides to fold in the ribbon conformation. However, with the introduction of both key structural features, the propensity to stay in the ribbon conformation gradually shifts toward the globular conformation. It is perhaps of evolutionary interest that these two structural features were retained in the toxins' structure so as to favor the formation of receptor specific ligands of the appropriate conformation.

ImI conotoxin has been identified as a signature ligand for *Aplysia* AChBP, which is a well-established structural and functional surrogate of human nicotinic acetylcholine receptor isolated from salt water mollusk *Aplysia californica*. The highly specific neurotoxic peptide, isolated from a vermivorous cone snail *Conus imperialis*, has been shown to possess a 16 000-fold preference to *Aplysia* AChBP (A-AChBP), over *Lymnaea* AChBP isolated from a fresh water mollusk *Lymnaea stagnalis* (*48*).

Despite the identical sequence, the non-native (ribbon and beaded) conformations of ImI conotoxin showed over 300-fold reduction in binding affinity with A-AChBP as compared with the native globular form. A conformational rearrangement of the C-loop at the subunit interface occurs during binding of the conotoxin to A-AChBP (*13*). We compared the conformational differences in the interaction segment of globular and ribbon forms to that of the bound conotoxin. The solution structure of ImI conotoxin (PDB ID 1IM1) overlaid with bound ImI conotoxin (from PDB ID 2BYP) to give a backbone rmsd of 0.79 Å, suggesting a slight conformational rearrangement between the two conformational states. The ribbon analogue of the ImI P6 Acid variant was compared in a pairwise backbone comparison with the crystal structure of ImI conotoxin complexed with the A-AChBP (2BYP). The region between Ser4−Cys8 of the first intercysteine loop 1 overlaid with an rmsd of 0.72 Å. This matching overlay occurs despite the poor backbone comparison of 3.66 Å for the whole molecule. The overlay improved to 0.28 Å when the region was limited to Asp5-Pro6-Arg7 triad. In the crystal structure of A-AChBP complexed with native ImI conotoxin, it was noted the region of Asp5−Arg7 tripeptide is deeply anchored into the binding pocket of the AChBP, and all three residues form critical stabilizing contacts either intramolecularly or with the side chains in the binding pocket (*48*). These results accord with the previous findings by Hansen et al. that the Asp5-Pro6-Arg7 triad is the major binding determinant responsible for its affinity to AChBP. Trp10 of the second intercysteine loop was also noted to establish extensive interactions with Arg79, Val108, Met116, and Arg59 of A-AChBP's binding pocket (*13*, *48*). A backbone comparison of the segment between Cys8−Cys12 revealed a poor overlay of 2.36 Å and a misaligned Trp10 indole side chain as illustrated in Figure 8A. The side chain of the neighboring Arg11 residue protrudes toward the AChBP subunit interface of the binding site (Figure 8B), possibly hindering entry of the ImI conotoxin into the AChBP binding site. It is likely that the critical region between Asp5 to Trp10 undergoes a significant degree of conformational rearrangement before forming a

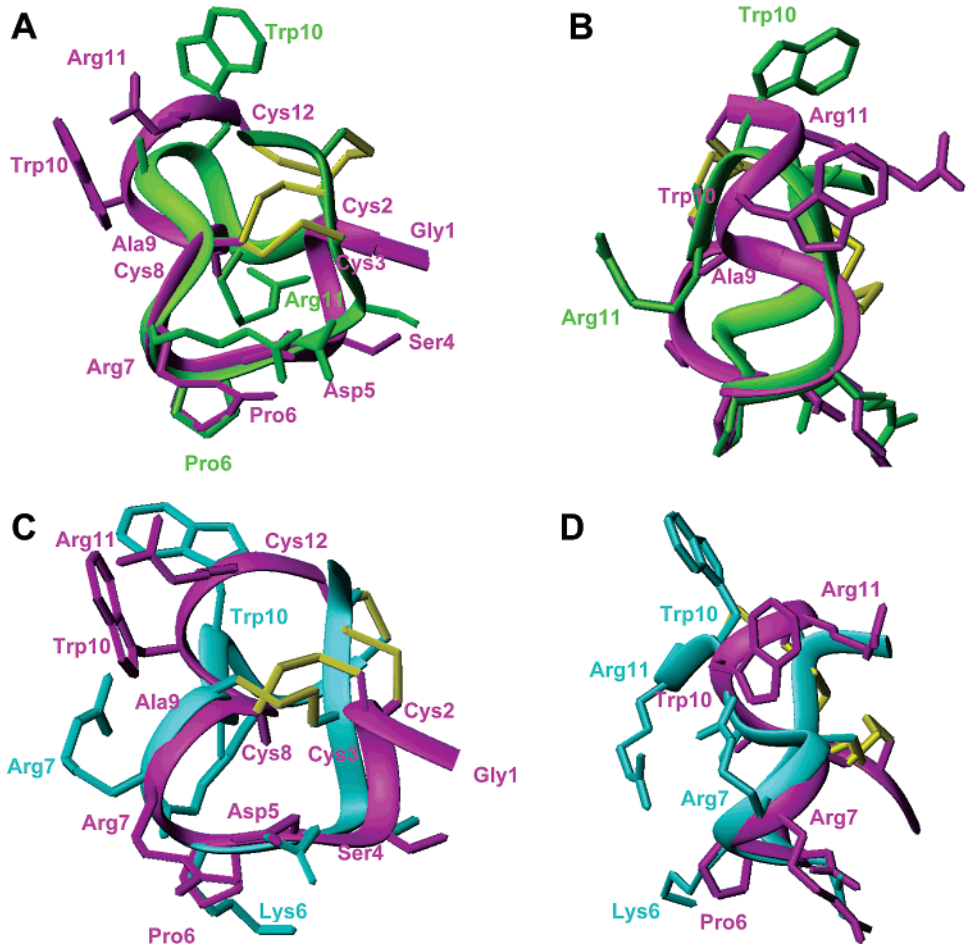

FIGURE 8: Comparison of structures. ImI P6 Amide (PDB ID 1IM1) compared with the averaged calculated solution structure of ImI P6 Acid ribbon conformation (A, B), and ImI K6 Acid ribbon conformation (C, D). ImI P6 Amide globular conformation, ImI P6 Acid ribbon conformation, and ImI K6 Acid ribbon conformation are presented in magenta, green, and cyan, respectively.

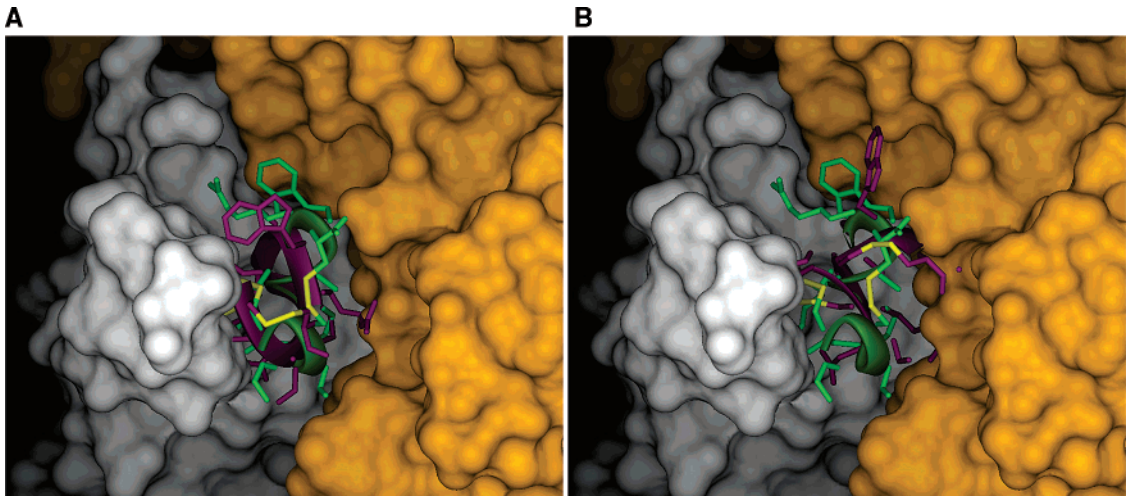

FIGURE 9: Comparison of structures with bound conotoxin ImI P6 Amide. ImI K6 Acid ribbon (panel A) and ImI P6 Acid ribbon (panel B) averaged conformations are overlaid with the globular conformation of ImI P6 Amide (PDB ID 2BYP, ImI P6 Amide presented in green) bound to A-AChBP. C-alpha atoms of amino acid residues 5−7 were used as basis for the overlay.

stable complex with A-AChBP. The decrease in affinity of ImI P6 Acid ribbon conformer is, thus, a likely result of dissimilar orientations of Trp10's indole ring and the overall backbone conformation of second intercysteine loop, thereby culminating to the 200-fold reduction in binding affinity of the ImI P6 Acid analogue. Through the superposition of the ribbon conformation of the ImI P6 Acid variant with the bound ImI conotoxin to the AChBP binding site, Figure 9 illustrates the structural differences between the ImI P6 Acid variant with the native toxin.

The ImI K6 Acid ribbon conformer having incorporated most structural changes in its sequence was expected to have the weakest binding affinity among the variants analyzed. In view of the charged aliphatic side chain that protrudes out of the crucial binding region between residue 4 to 8 of the first intercysteine loop, it is not surprising when ImI K6

Acid ribbon conformer presents a K_d of weaker than 0.5 mM. The disruption of the major binding determinant may explain the near complete loss of affinity despite a similar overall conformation of this region (Ser4−Cys8 overlays with 0.58 Å rmsd as shown in Figure 8B). The decrease in activity of this variant is possibly amplified by poorly oriented side chains of Arg11 of the second intercysteine loop, rendering severe steric hindrance to the binding pocket (Figures 8C,D and 9B).

In this study, we have shown that substitution of Pro-6 from the sequence of ImI conotoxin has not just disrupted the in vitro folding patterns of the toxin but also elicits a severe reduction in the binding affinity of the peptide analogues to the receptor A-AChBP. We broadly infer from the results that the presence of proline residue at position 6 of the sequence is important in defining the constrained helical secondary structure of the peptide backbone and thus critically affecting the binding affinity. The defined backbone conformation is buttressed with the conserved disulfide linkages (C_{1-3}, C_{2-4}) in defining the globular conformation. C-Terminal amidation not only acts as a conformational switch in the folding of ImI conotoxin (*12*) but also appreciably influences the binding affinity of the variants, for its absence can reduce the affinity approximately 10-fold.

ACKNOWLEDGMENT

Tse Siang Kang acknowledges the Singapore Millennium Foundation for granting the research scholarship, and the National University of Singapore for granting the NUS research scholarship for the period of July 2002 to July 2004. The authors thank the Sophisticated Instrument Facility at Indian Institute of Science, Bangalore, India, and the Chemical and Molecular Analysis Center, Department of Chemistry at National University of Singapore, for allowing the use of the NMR spectrometers.

SUPPORTING INFORMATION AVAILABLE

Chromatographic coelution profiles, ^{1}H NMR spectra, mass spectrometry data, and superimposition of calculated structures. This material is available free of charge via the Internet at http://pubs.acs.org.

REFERENCES

1. McIntosh, J. M., Santos, A. D., and Olivera, B. M. (1999) Conus peptides targeted to specific nicotinic acetylcholine receptor subtypes, *Annu. Rev. Biochem. 68*, 59−88.
2. Arias, H. R. and Blanton, M. P. (2000) Alpha-conotoxins, *Int. J. Biochem. Cell Biol. 32*, 1017−1028.
3. Terlau, H., and Olivera, B. M. (2004) Conus venoms: a rich source of novel ion channel-targeted peptides, *Physiol Rev. 84*, 41−68.
4. Gehrmann, J., Alewood, P. F., and Craik, D. J. (1998) Structure determination of the three disulfide bond isomers of alpha-conotoxin GI: A model for the role of disulfide bonds in structural stability, *J. Mol. Biol. 278*, 401−415.
5. Zhang, R. M., and Snyder, G. H. (1991) Factors governing selective formation of specific disulfides in synthetic variants of alpha-conotoxin, *Biochemistry, 30*, 11343−11348.
6. Carlier, E., Fajloun, Z., Mansuelle, P., Fathallah, M., Mosbah, A., Oughideni, R., Sandoz, G., Di Luccio, E., Geib, S., Regaya, I., Brocard, J., Rochat, H., Darbon, H., Devaux, C., Sabatier, J. M., and de Waard, M. (2001) Disulfide bridge reorganization induced by proline mutations in maurotoxin, *FEBS Lett. 489*, 202−207.
7. Kini, R. M., and Evans, H. J. (1995) A novel approach to the design of potent bioactive peptides by incorporation of proline brackets: Antiplatelet effects of Arg-Gly-Asp peptides, *FEBS Lett. 375*, 15−17.
8. Luo, S., Kulak, J. M., Cartier, G. E., Jacobsen, R. B., Yoshikami, D., Olivera, B. M., and McIntosh, J. M. (1998) Alpha-conotoxin AuIB selectively blocks alpha3 beta4 nicotinic acetylcholine receptors and nicotine-evoked norepinephrine release, *J. Neurosci. 18*, 8571−8579.
9. Balaji, R. A., Ohtake, A., Sato, K., Gopalakrishnakone, P., Kini, R. M., Seow, K. T., and Bay, B. H. (2000) Lambda-conotoxins, a new family of conotoxins with unique disulfide pattern and protein folding. Isolation and characterization from the venom of *Conus marmoreus*, *J. Biol. Chem. 275*, 39516−39522.
10. McIntosh, J. M., Corpuz, G. O., Layer, R. T., Garrett, J. E., Wagstaff, J. D., Bulaj, G., Vyazovkina, A., Yoshikami, D., Cruz, L. J., and Olivera, B. M. (2000) Isolation and characterization of a novel conus peptide with apparent antinociceptive activity, *J. Biol. Chem. 275*, 32391−32397.
11. Sharpe, I. A., Gehrmann, J., Loughnan, M. L., Thomas, L., Adams, D. A., Atkins, A., Palant, E., Craik, D. J., Adams, D. J., Alewood, P. F., and Lewis, R. J. (2001) Two new classes of conopeptides inhibit the alpha1-adrenoceptor and noradrenaline transporter, *Nat. Neurosci. 4*, 902−907.
12. Kang, T. S., Vivekanandan, S., Jois, S. D., and Kini, R. M. (2005) Effect of C-terminal amidation on folding and disulfide-pairing of alpha-conotoxin ImI, *Angew. Chem. Int. Ed Engl. 44*, 6333−6337.
13. Hansen, S. B., Sulzenbacher, G., Huxford, T., Marchot, P., Taylor, P., and Bourne, Y. (2005) Structures of Aplysia AChBP complexes with nicotinic agonists and antagonists reveal distinctive binding interfaces and conformations, *EMBO J. 24*, 3635−3646.
14. Celie, P. H., Kasheverov, I. E., Mordvintsev, D. Y., Hogg, R. C., van Nierop, P., van Elk, R., Rossum-Fikkert, S. E., Zhmak, M. N., Bertrand, D., Tsetlin, V., Sixma, T. K., and Smit, A. B. (2005) Crystal structure of nicotinic acetylcholine receptor homolog AChBP in complex with an alpha-conotoxin PnIA variant, *Nat. Struct. Mol. Biol. 12*, 582−588.
15. Bax, A. D., and Davis, D. G. (1985) MLEV-17-based two-dimensional homonuclear magnetization transfer spectroscopy, *J. Magn. Reson. 65*, 355−360.
16. Bax, A. D., and Davis, D. G. (1985) Practical aspects of two-dimensional transverse NOE spectroscopy, *J. Magn. Reson. 63*, 207−213.
17. Piotto, M., Saudek, V., and Sklenar, V. (1992) Gradient-tailored excitation for single-quantum NMR spectroscopy of aqueous solutions, *J. Biomol*. NMR *2*, 661−665.
18. Wuthrich, K. (1986) *NMR of Proteins and Nucleic Acids*; Wiley: New York.
19. Nicke, A., Loughnan, M. L., Millard, E. L., Alewood, P. F., Adams, D. J., Daly, N. L., Craik, D. J., and Lewis, R. J. (2003) Isolation, structure, and activity of GID, a novel alpha 4/7-conotoxin with an extended N-terminal sequence, *J. Biol. Chem. 278*, 3137−3144.
20. Broxton, N. M., Down, J. G., Gehrmann, J., Alewood, P. F., Satchell, D. G., and Livett, B. G. (1999) Alpha-conotoxin ImI inhibits the alpha-bungarotoxin-resistant nicotinic response in bovine adrenal chromaffin cells, *J. Neurochem. 72*, 1656−1662.
21. Ellison, M., McIntosh, J. M., and Olivera, B. M. (2003) Alpha-conotoxins ImI and ImII. Similar alpha 7 nicotinic receptor antagonists act at different sites, *J. Biol. Chem. 278*, 757−764.
22. Gehrmann, J., Daly, N. L., Alewood, P. F., and Craik, D. J. (1999) Solution structure of alpha-conotoxin ImI by 1H nuclear magnetic resonance, *J. Med. Chem. 42*, 2364−2372.
23. Gouda, H., and Hirono, S. (1999) Solution structure of alpha-conotoxin ImI determined by two-dimensional NMR spectroscopy *Biochim. Biophys. Acta 1431*, 384−394.
24. Johnson, D. S., Martinez, J., Elgoyhen, A. B., Heinemann, S. F., and McIntosh, J. M. (1995) Alpha-Conotoxin ImI exhibits subtype-specific nicotinic acetylcholine receptor blockade: preferential inhibition of homomeric alpha 7 and alpha 9 receptors, *Mol. Pharmacol. 48*, 194−199.
25. Lamthanh, H., Jegou-Matheron, C., Servent, D., Menez, A., and Lancelin, J. M. (1999) Minimal conformation of the alpha-conotoxin ImI for the alpha7 neuronal nicotinic acetylcholine receptor recognition: correlated CD, NMR and binding studies, *FEBS Lett. 454*, 293−298.
26. Maslennikov, I. V., Shenkarev, Z. O., Zhmak, M. N., Ivanov, V. T., Methfessel, C., Tsetlin, V. I., and Arseniev, A. S. (1999) NMR spatial structure of alpha-conotoxin ImI reveals a common scaffold in snail and snake toxins recognizing neuronal nicotinic acetylcholine receptors, *FEBS Lett. 444*, 275−280.

27. McIntosh, J. M., Yoshikami, D., Mahe, E., Nielsen, D. B., Rivier, J. E., Gray, W. R., and Olivera, B. M. (1994) A nicotinic acetylcholine receptor ligand of unique specificity, alpha-conotoxin ImI, *J. Biol. Chem. 269*, 16733−16739.
28. Nielsen, J. S., Buczek, P., and Bulaj, G. (2004) Cosolvent-assisted oxidative folding of a bicyclic alpha-conotoxin ImI, *J. Pept. Sci. 10*, 249−256.
29. Quiram, P. A., and Sine, S. M. (1998) Structural elements in alpha-conotoxin ImI essential for binding to neuronal alpha7 receptors, *J. Biol. Chem. 273*, 11007−11011.
30. Quiram, P. A., and Sine, S. M. (1998) Identification of residues in the neuronal alpha7 acetylcholine receptor that confer selectivity for conotoxin ImI, *J. Biol. Chem. 273*, 11001−11006.
31. Quiram, P. A., Jones, J. J., and Sine, S. M. (1999) Pairwise interactions between neuronal alpha7 acetylcholine receptors and alpha-conotoxin ImI, *J. Biol. Chem. 274*, 19517−19524.
32. Rogers, J. P., Luginbuhl, P., Shen, G. S., McCabe, R. T., Stevens, R. C., and Wemmer, D. E. (1999) NMR solution structure of alpha-conotoxin ImI and comparison to other conotoxins specific for neuronal nicotinic acetylcholine receptors, *Biochemistry 38*, 3874−3882.
33. Utkin, Y. N., Zhmak, M. N., Methfessel, C., and Tsetlin, V. I. (1999) Aromatic substitutions in alpha-conotoxin ImI. Synthesis of iodinated photoactivatable derivative, *Toxicon 37*, 1683−1695.
34. Bellizzi, J. J., III, Widom, J., Kemp, C., Lu, J. Y., Das, A. K., Hofmann, S. L., and Clardy, J. (2000) The crystal structure of palmitoyl protein thioesterase 1 and the molecular basis of infantile neuronal ceroid lipofuscinosis, *Proc. Natl. Acad. Sci. U.S.A. 97*, 4573−4578.
35. Brejc, K., van Dijk, W. J., Klaassen, R. V., Schuurmans, M., van Der, O. J., Smit, A. B., and Sixma, T. K. (2001) Crystal structure of an ACh-binding protein reveals the ligand-binding domain of nicotinic receptors, *Nature 411*, 269−276.
36. Carugo, O., Cemazar, M., Zahariev, S., Hudaky, I., Gaspari, Z., Perczel, A., and Pongor, S. (2003) Vicinal disulfide turns, *Protein Eng. 16*, 637−639.
37. Ghosh, M., Anthony, C., Harlos, K., Goodwin, M. G., and Blake, C. (1995) The refined structure of the quinoprotein methanol dehydrogenase from Methylobacterium extorquens at 1.94 Å, *Structure 3*, 177−187.
38. Hunter, H. N., Fulton, D. B., Ganz, T., and Vogel, H. J. (2002) The solution structure of human hepcidin, a peptide hormone with antimicrobial activity that is involved in iron uptake and hereditary hemochromatosis, *J. Biol. Chem. 277*, 37597−37603.
39. Keitel, T., Diehl, A., Knaute, T., Stezowski, J. J., Hohne, W., and Gorisch, H. (2000) X-ray structure of the quinoprotein ethanol dehydrogenase from Pseudomonas aeruginosa: basis of substrate specificity, *J. Mol. Biol. 297*, 961−974.
40. Teplyakov, A., Polyakov, K., Obmolova, G., Strokopytov, B., Kuranova, I., Osterman, A., Grishin, N., Smulevitch, S., Zagnitko, O., and Galperina, O. (1992) Crystal structure of carboxypeptidase T from Thermoactinomyces vulgaris, Eur. *J. Biochem. 208*, 281−288.
41. Wang, X., Connor, M., Smith, R., Maciejewski, M. W., Howden, M. E., Nicholson, G. M., Christie, M. J., and King, G. F. (2000) Discovery and characterization of a family of insecticidal neurotoxins with a rare vicinal disulfide bridge, *Nat. Struct. Biol. 7*, 505−513.
42. Yoon, H. J., Hashimoto, W., Miyake, O., Murata, K., and Mikami, B. (2001) Crystal structure of alginate lyase A1-III complexed with trisaccharide product at 2.0 Å resolution, *J. Mol. Biol. 307*, 9−16.
43. Zeng, H., Moise, L., Grant, M. A., and Hawrot, E. (2001) The solution structure of the complex formed between alpha-bungarotoxin and an 18-mer cognate peptide derived from the alpha 1 subunit of the nicotinic acetylcholine receptor from Torpedo californica, *J. Biol. Chem. 276*, 22930−22940.
44. Wishart, D. S., Sykes, B. D., and Richards, F. M. (1992) The chemical shift index: a fast and simple method for the assignment of protein secondary structure through NMR spectroscopy, *Biochemistry 31*, 1647−1651.
45. Kang, T. S., Jois, S. D., and Kini, R. M. (2006) Solution structures of two structural isoforms of CMrVIA chi/lambda-conotoxin, *Biomacromolecules 7*, 2337−2346.
46. Buczek, O., Olivera, B. M., and Bulaj, G. (2004) Propeptide does not act as an intramolecular chaperone but facilitates protein disulfide isomerase-assisted folding of a conotoxin precursor, *Biochemistry 43*, 1093−1101.
47. Loughnan, M. L., Nicke, A., Jones, A., Adams, D. J., Alewood, P. F., and Lewis, R. J. (2004) Chemical and functional identification and characterization of novel sulfated alpha-conotoxins from the cone snail Conus anemone, *J. Med. Chem. 47*, 1234−1241.
48. Hansen, S. B., Talley, T. T., Radic, Z., and Taylor, P. (2004) Structural and ligand recognition characteristics of an acetylcholine-binding protein from Aplysia californica, *J. Biol. Chem. 279*, 24197−24202.
49. Loughnan, M., Bond, T., Atkins, A., Cuevas, J., Adams, D. J., Broxton, N. M., Livett, B. G., Down, J. G., Jones, A., Alewood, P. F., and Lewis, R. J. (1998) Alpha-conotoxin EpI, a novel sulfated peptide from Conus episcopatus that selectively targets neuronal nicotinic acetylcholine receptors, *J. Biol. Chem. 273*, 15667−15674.
50. Fainzilber, M., Hasson, A., Oren, R., Burlingame, A. L., Gordon, D., Spira, M. E., and Zlotkin, E. (1994) New mollusc-specific alpha-conotoxins block Aplysia neuronal acetylcholine receptors, *Biochemistry 33*, 9523−9529.
51. Cartier, G. E., Yoshikami, D., Gray, W. R., Luo, S., Olivera, B. M., and McIntosh, J. M. (1996) A new alpha-conotoxin which targets alpha3beta2 nicotinic acetylcholine receptors, *J. Biol. Chem. 271*, 7522−7528.
52. Martinez, J. S., Olivera, B. M., Gray, W. R., Craig, A. G., Groebe, D. R., Abramson, S. N., and McIntosh, J. M. (1995) Alpha-conotoxin EI, a new nicotinic acetylcholine receptor antagonist with novel selectivity, *Biochemistry 34*, 14519−14526.
53. McIntosh, J. M., Dowell, C., Watkins, M., Garrett, J. E., Yoshikami, D., and Olivera, B. M. (2002) Alpha-conotoxin GIC from Conus geographus, a novel peptide antagonist of nicotinic acetylcholine receptors, *J. Biol. Chem. 277*, 33610−33615.
54. Sandall, D. W., Satkunanathan, N., Keays, D. A., Polidano, M. A., Liping, X., Pham, V., Down, J. G., Khalil, Z., Livett, B. G., and Gayler, K. R. (2003) A novel alpha-conotoxin identified by gene sequencing is active in suppressing the vascular response to selective stimulation of sensory nerves in vivo, *Biochemistry 42*, 6904−6911.
55. Azam, L., Dowell, C., Watkins, M., Stitzel, J. A., Olivera, B. M., and McIntosh, J. M. (2005) Alpha-conotoxin BuIA, a novel peptide from Conus bullatus, distinguishes among neuronal nicotinic acetylcholine receptors, *J. Biol. Chem. 280*, 80−87.
56. Chi, S. W., Kim, D. H., Olivera, B. M., McIntosh, J. M., and Han, K. H. (2006) Solution conformation of a neuronal nicotinic acetylcholine receptor antagonist alpha-conotoxin OmIA that discriminates alpha3 vs. alpha6 nAChR subtypes, *Biochem. Biophys. Res. Commun. 345*, 248−254.
57. Gray, W. R., Luque, A., Olivera, B. M., Barrett, J., and Cruz, L. J. (1981) Peptide toins from Conus geographus venom, *J. Biol. Chem. 256*, 4734−4740.
58. Zafaralla, G. C., Ramilo, C., Gray, W. R., Karlstrom, R., Olivera, B. M., and Cruz, L. J. (1988) Phylogenetic specificity of cholinergic ligands: alpha-conotoxin SI, *Biochemistry 27*, 7102−7105.

BI061969O